HHS Public Access

Author manuscript

ACS Appl Mater Interfaces. Author manuscript; available in PMC 2016 August 27.

Published in final edited form as:

ACS Appl Mater Interfaces. 2016 March ; 8(12): 7691–7708. doi:10.1021/acsami.6b01160.

Self-Setting Calcium Phosphate Cements with Tunable Antibiotic Release Rates for Advanced Antimicrobial Applications

Shreya Ghosh, **Victoria Wu**, **Sebastian Pernal**, and **Vuk Uskoković***

Advanced Materials and Nanobiotechnology Laboratory, Department of Bioengineering, University of Illinois, Chicago, Illinois 60607, United States

Abstract

Osteomyelitis, an infectious disease predominantly tied to poor sanitary conditions in underdeveloped regions of the world, is in need of inexpensive, easily in situ synthesizable and administrable materials for its treatment. The results of this study stem from the attempt to create one such affordable and minimally invasive therapeutic platform in the form of a self-setting, injectable cement with a tunable drug release profile, composed of only nanoparticulate hydroxyapatite, the synthetic version of the bone mineral. Cements comprised two separately synthesized hydroxyapatite powders, one of which, HAP2, was precipitated abruptly, retaining the amorphous nature longer, and the other one of which, HAP1, was precipitated at a slower rate, more rapidly transitioning to the crystalline structure. Cements were made with four different weight ratios of the two hydroxyapatite components: 100/ 0, 85/15, 50/50, and 0/100 with respect to HAP1 and HAP2. Both the setting and the release rates measured on two different antibiotics, vancomycin and ciprofloxacin, were controlled using the weight ratio of the two hydroxyapatite components. Various inorganic powder properties were formerly used to control drug release, but here we demonstrate for the first time that the kinetics of the mechanism of formation of a solid compound can be controlled to produce tunable drug release profiles. Specifically, it was found that the longer the precursor calcium phosphate component of the cement retains the amorphous nature of the primary precipitate, the more active it was in terms of speeding up the diffusional release of the adsorbed drug. The setting rate was, in contrast, inversely proportional to the release rate and to the content of this active hydroxyapatite component, HAP2. The empirical release profiles were fitted to a set of equations that could be used to tune the release rate to the therapeutic occasion. All of the cements loaded with vancomycin or ciprofloxacin inhibited the growth of Gram-positive *Staphylococcus aureus* and Gram-negative *Escherichia coli* and *Pseudomonas aeruginosa* in both agar diffusion assays and broth dilution tests with intensities either comparable to the antibiotic per se, as in the case of ciprofloxacin, or even larger than the antibiotic alone, as in the case of vancomycin. Interestingly, even the pure cements exhibited an antibacterial effect ranging from moderate to strong, while demonstrating high levels of biocompatibility with osteoclastic RAW264.7 cells and only slightly affecting the viability of the osteoblastic MC3T3-E1 cells, in direct proportion with the amount of the more active hydroxyapatite component in the cements. This antibacterial effect was especially noticeable against Gram-negative bacteria, where the growth inhibition by the cements was comparable to or

***Corresponding Author**. vuk21@yahoo.com.

The authors declare no competing financial interest.

even stronger than that of the pure antibiotics. The antibiofilm assay against *P. aeruginosa* biofilms reiterated the antibiotic effectiveness of pure, antibiotic-free cements. That the carrier per se, composed of a nontoxic, easily prepared, bone mineral composite, can exhibit a strong antibacterial effect even in the absence of an antibiotic drug is an insight highly relevant in view of the rising resistance of an array of pathogens to traditional antibiotic therapies and the demands for the timely development of suitable alternatives.

Graphical abstract

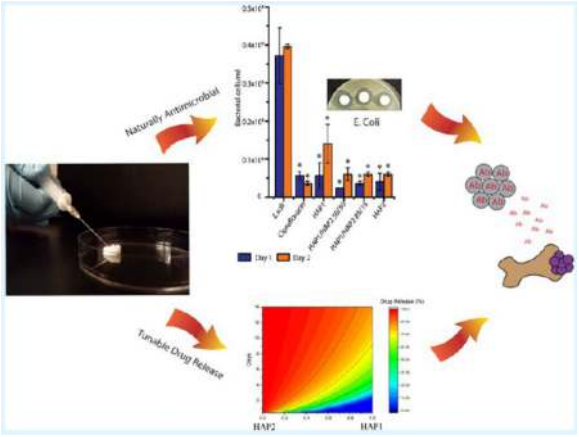

Keywords

antibacterial; bone graft; calcium phosphate; hydroxyapatite; tunable release; self-setting cement

1. INTRODUCTION

Osteomyelitis, a bone disease whose prevalence is expected to increase in direct proportion with the projected aging of the average population on Earth, is still predominantly treated in the clinic with systemic antibiotic therapies.[1] Not only is this method prone to induce multiple side effects because of the systemic distribution of the drug, but the drug distributed by these means also has a difficult time crossing zones of impaired vascularization and biofilm formation and reaching the infected tissue. Bone, namely, is an organ well shielded from the external pathogens. However, this shielding effect becomes a double-edged sword when therapeutic molecules are attempted to be administered thereto through the bloodstream. A diminished concentration of the antibiotic in the area of infection not only can have little effect in inhibiting or annihilating the population of the pathogen but can also lead to a rise in bacterial resistance to the antibiotic therapy,[2] an effect that currently poses a global threat to the health of the humankind.[3] Systemic antibiotic therapies, be they oral or parenteral, are also not very cost-effective and require repetitive administration at high dosages in order to maintain the concentration of the antibiotic in the blood and at the target area at the therapeutically effective level. Sustained and locally distributable release platforms are thus greatly favored over the traditional therapies.

In this study, we focus on the development of one such osteogenic carrier capable of releasing the antibiotics vancomycin or ciprofloxacin at a tunable rate ranging from hours to weeks. The need for a drug carrier with tunable release rates is justified by the fact that bone is a material whose density, vascularization, and remodeling rates vary more than in any other organ as one moves from its edge to the center. Namely, as one shifts from the dense cortical surface to the lighter trabecular interior and then to the soft bone marrow, porosity, vascularization, and remodeling rates increase, justifying the necessity for one such platform whose release rates could be precisely and easily tailored to the right location and geometry of defects within the bone.

At the same time, tissue necrosis, necessitating surgical debridement and frequently causing biomechanical failure and unaesthetic disfigurement, are common outcomes of chronic osteomyelitis.[4–6] Incentives thus exist to develop therapeutic materials that would assist in the regeneration of the tissue following eradication of the infection source. In this study, we have used hydroxyapatite (HAP), the most thermodynamically stable form of calcium phosphate and the sole mineral component of natural bone, as a drug delivery carrier. Calcium phosphates, including HAP, are biocompatible, bioactive and osteoconductive.[7] They have also been shown to accelerate the formation of new bone and present the most natural choice for the replacement of diseased bone tissues,[7–9] conforming to the ancient Latin maxim “similia similibus curantur”, or “like is cured by like”.

In addition to being osteogenic, an ideal bone replacement material is supposed to possess self-setting properties. A self-setting material has the potential to easily conform to the shape of the defect as well as be directly injectable into the affected area, thus circumventing the need for open surgical intervention, diminishing the overall cost of the therapy, minimizing the size of the wound and speeding up the healing process. Calcium phosphate can be readily prepared in the form of self-setting cements and the injectable formulations of such cements have been approved for clinical use in the United States and the European Union since 2009. Alongside their excellent moldability and osseointegration, calcium phosphate cements take advantage of the endothermic nature of precipitation of calcium phosphates,[10] contrasting the exothermic character of most cement solidification processes, whereby heat detrimental to cement/tissue integration is being released. Although the setting kinetics of calcium phosphate cements can be controlled in situ using parameters such as the particle size,[11] liquid-to-powder ratio,[12] pH,[13] temperature,[14] or the concentration of setting promoters,[15] the kinetics of the drug release from these cements has not been made tunable yet in the true sense of the word. In this study, we demonstrate that the release kinetics could be made tunable in situ by controlling the weight ratio between the two, interestingly, chemically, morphologically and crystallographically identical calcium phosphate components. The composition and the setting mechanism of the cements developed in this study is also new, given that they circumvent dicalcium phosphates as intermediates and involve the direct transition of the amorphous to crystalline HAP. Although calcium phosphate cements may seem as an exhausted subject for research, belonging more to the past than to the future, here we demonstrate that exciting new potentialities still lie dormant in them and possibly herald their renaissance in the realm of tissue engineering.

Finally, with osteomyelitis still being a disease found mostly in underdeveloped nations,[16,17] the need to create a low-cost, easily in situ synthesizable option for its treatment, affordable to people from all economic backgrounds, cannot be overemphasized. Expensive polymers, chemical conjugations, surfactants, growth factors, and other biomolecular components, alongside complex preparatory setups are not readily available in regions where osteomyelitis is endemic and were thus systematically avoided in this study in favor of readily available components and simple precipitation chemistries that could be easily replicated in the most basic of laboratory settings. Thus, the aim of this study was to fabricate a tunable drug release platform with controllable setting properties using only calcium phosphate, a material that epitomizes Nature's finding perfections solely in perfect imperfections.[18] We also demonstrate for the first time that the drug release rates could be made tunable depending on the phase transformation pathways leading to the final microstructures of the powders combined in self-setting cements. With such an approach, an attempt was made to implicitly point out the remarkable and largely unexplored potentials of the single compound comprising the mineral component of all hard tissues in the human body except for the calcite-containing portions of the inner ear: calcium phosphate.

2. MATERIALS AND METHODS

2.1. Synthesis of Drug-Loaded Calcium Phosphate Cements

The self-setting cements prepared in this study were composed of one or more of the three different and separately synthesized types of hydroxyapatite (HAP), termed here as HAP1, HAP2, and HAP3.

To make HAP1, 400 mL of 0.06 M aqueous solution of $NH_4H_2PO_4$ containing 25 mL 28% NH_4OH was added dropwise to the same volume of 0.1 M aqueous solution of $Ca(NO_3)_2$ (Fisher Scientific) containing 50 mL 28% NH_4OH (Sigma-Aldrich), vigorously stirred with a magnetic bar (400 rpm) and kept on a plate heated to 50 °C. After the addition of $NH_4H_2PO_4$ (Fisher Scientific) was complete, the suspension was brought to boiling, then immediately removed from the heater and air cooled to room temperature. Stirring was suspended, and the precipitate together with its parent solution, the final pH of which was 10.6, were left to age in atmospheric conditions for 24 h. After the given time, the precipitate was washed once with deionized (DI) H_2O, centrifuged (10 s at 3500 rpm), and let dry overnight in a vacuum oven (Accu Temp-19, Across International) ($p = -20$ mmHg) at 80 °C.

HAP2 was formed by abruptly adding a solution containing 100 mL 0.5 M $Ca(NO_3)_2$ and 7 mL 28% NH_4OH into a solution comprising 100 mL 0.2 M $NH_4H_2PO_4$ and 4 mL 28% NH_4OH. The fine precipitate formed upon mixing was aged for 15 s, before it was collected, centrifuged, washed with 0.14 w/v% NH_4OH, centrifuged again, and dried overnight at low pressure ($p = -20$ mmHg) and room temperature. The pH of the supernatant following the precipitation reaction was 9.3. An additional phase, HAP3, was prepared for comparison purposes by mixing 400 mL 0.33 M $Ca(NO_3)_2$ and 400 mL 0.25 M $NH_4H_2PO_4$ containing 10 mL 28% NH_4OH, with all the other conditions being the same as for the synthesis of HAP1. The pH of the supernatant following the precipitation reaction was 5.2.

The self-setting cements consisted of a solid and a liquid phase, the former comprising HAP1 and HAP2 mixed in different weight ratios (100/0, 85/15, 50/50 and 0/100) and the latter consisting of 2 wt % aqueous solution of Na_2HPO_4. To make the drug-loaded HAP1 and HAP2, either vancomycin (M.P. Biomedicals) or ciprofloxacin (Acros Organics) were added to the HAP powder mixture in a 50 mL Falcon tube. This was followed by mixing using a digital vortex mixer (Fisher Scientific) for 5 min at 2000 rpm, after which 2 wt % Na_2HPO_4 (aq.)[19] (Sigma-Aldrich) was added dropwise to the solid mixture. Following this addition, the cement was again vortex mixed for 5 min at 2000 rpm. A constant solid-to-liquid ratio of 1.782 g/mL was employed, while the amount of vancomycin or ciprofloxacin in each sample equaled 2.5 wt %. Table 1 shows the composition of the solid phase of the samples.

2.2. Structural and Morphological Characterization

Scanning electron microscopy (SEM) studies were carried out on a JEOL JSM 6320F-FESEM operated at 4.2 kV voltage and 8 μA beam current. Sample preparation involved depositing powders or pastes on clean aluminum stubs using the carbon tape and subsequently sputter-coating them with gold to reduce the charging effects. X-ray diffraction (XRD) was carried out on a Bruker D2 Phaser diffractometer using polychromatic Cu as the irradiation source. Kβ line was stripped off with an inbuilt filter, whereas Kα2 line was stripped off manually. The step size was 0.01°, with 1 s of sample irradiation per step. Particle size distribution histograms for the different types of cements and HAP precursors were obtained from their corresponding scanning electron micrographs using ImageJ (NIH, Bethesda, MD) and the sample size of 200–1000 particles. Porosity was measured using a method reported earlier.[20] Paste samples were filled into cylindrical molds of different sizes and allowed to set at 37 °C, after which they were taken out and cured at 100 °C for 15 min. Once cured, the dimensions and weights of the samples were measured in triplicates. This allowed us to calculate the experimental densities of samples, the comparison of which against the theoretical densities of HAP1 and HAP2 (3.156 and 2.895 g/cm^3, respectively[21,22]) led to the estimate of porosity.

2.3. Setting Time Determination

The setting time of the samples was divided into two categories, namely, the initial setting time and the final setting time. The measurements were done in accordance with ISO 1566.[23] The standard Vicat needle method was used on samples placed in 47 mm Petri dishes (Fisherbrand) and incubated at 37 °C. The cement was considered initially set when the needle (30G Hypodermic Disposable Needles, EXEL International) made a slight circular indentation on the surface of the sample but was far from the bottom. The final setting time was noted when the needle failed to make any visible indentation on the sample surface.[24] To determine the setting time variations based on the sample volume, different volumes (50, 100, 150, 200, and 280 μL), which were equivalent to different weights (0.089, 0.178, 0.267, 0.356, and 0.5 g, respectively), were incubated at 37 °C in 47 mm Petri dishes and their final setting times were noted by the same method as mentioned previously.

2.4. In Vitro Drug Release

The drug-loaded cements were allowed to completely set before they were placed in 50 mL of phosphate buffered saline (PBS) in closed conical tubes and incubated at 37 °C and 50 rpm rotation perpendicular to the cylinder axis. The drug release rates from bone cements were determined in duplicates by taking 1 mL PBS after 0.167 h (10 min), 0.5, 1, 2, 3, 4, 24 h and once every following day until 100% of the drug was released. The volume of the aliquoted solution was replaced each time with fresh PBS. The drug content was determined by measuring the corresponding absorbance on a UV/vis spectrophotometer (Nanodrop 2000, Thermo Scientific) at $\lambda = 200$ nm for vancomycin-containing samples and $\lambda = 270$ nm for ciprofloxacin-containing samples.

2.4.1. Parameter Fitting—The parameters of the equations modeling in vitro drug release were determined using the least-squares method. The two-variable drug release model was decided by first comparing the drug release to each variable separately and then directing a single, two-variable equation. Once the model was deduced, the parameters of the two-variable model were determined using the least-squares method as well.

2.5. Antibacterial Tests

Antibacterial tests of the bone cements were performed against *Staphylococcus aureus* ATCC 27661 (Carolina Biological Supply), a Gram-positive bacterium, and *Escherichia coli* ATCC 14948 (Carolina Biological Supply) and *Pseudomonas aeruginosa* ATCC 27853 (Carolina Biological Supply) as Gram-negative ones.

2.5.1. Agar Diffusion Assay—For the agar diffusion test, blood agar plates (Sigma Life Sciences) for *S. aureus* and nutrient agar (Sigma Life Sciences) plates for *E. coli* and *P. aeruginosa* were prepared. One hundred microliters of bacterial inoculation of each type was spread uniformly on the plates using plating beads. Subsequently, 25 μL of the cement samples, which contained 1.11 mg of the drug, were added to the plates and allowed to incubate overnight at 37 °C. All the samples for the agar diffusion test were analyzed in triplicates. The antibacterial efficacy of each antibiotic-loaded cement was compared to that of the antibiotic only (positive control) and to that of the cement containing no antibiotic (negative control).

2.5.2. Liquid Inoculation Assay—In the liquid inoculation test of the vancomycin-containing samples, a single colony of *S. aureus* cultured on a blood agar plate over a period of 24 h was stabbed with a pipet tip and placed in 5 mL of brain heart infusion broth (Sigma Life Sciences) and incubated overnight at 37 °C and 170 rpm. The same procedure was repeated for *P. aeruginosa* and *E. coli*, both of which were cultured on nutrient agar plates and were inoculated in 5 mL of nutrient broth (Sigma Life Sciences). Twenty-five microliters of each sample, containing 1.11 mg of the drug, were analyzed. All the samples for this assay were analyzed in duplicates. Each drug-loaded cement sample was compared to a set of three controls. The first control was termed standard; it contained 5 mL of the broth in which a single colony of bacteria was introduced and then incubated for 24 h. The second control was termed as the positive control, where the drug was added to the broth and the bacteria in order to assess the antibacterial efficacy of the drug without any carrier. The

third control was denoted as negative control where the bone cements without any drug were added to the broth and bacterial mixture, in order to determine the antibacterial efficacy of just the carrier.

2.5.3. Antibiofilm Assay—*P. aeruginosa* was grown overnight in Tryptic Soy Broth (Sigma-Aldrich) followed by resuspension in M9 minimal Media (Sigma Life Sciences) supplemented with 0.4%w/v D-(+)-Glucose (Sigma-Aldrich). The concentration of the bacteria was then adjusted to 1×10^7 CFU/ml. Ten microliters of a bone cement sample along with 90 μL of bacteria was then added to each well in a 96-well plate. After incubating for 24 h, each well was washed twice with 150 μL of PBS. An MTT assay was preformed using the Vybrant MTT Cell Proliferation Assay Kit (Molecular Probes) according to the manufacturer's instructions. All the samples for this assay were analyzed in triplicates.

2.6. Osteoclast Interaction

Mouse monocyte macrophage RAW264.7 cells were obtained from ATCC and cultured in Dulbecco's modified Eagle medium (DMEM) with 10 vol % FBS and 5 vol % antibiotic/antimycotic (streptomycin/penicillin/fungisone). RAW264.7 cells were seeded onto glass coverslips in 24-well plates at a concentration of 5.5×10^5 cells/well and allowed to differentiate for 9 days in the presence of 35 ng/mL of mRANKL and 10 μL/well of the self-setting bone cements. After the given period of time, the cells were stained for Tartrate-resistant acid phosphatase (TRAP) using a commercial acid phosphatase leucocyte kit (Sigma). After 1 week of incubation with the cements, the cells were washed thrice with PBS after removing the media. The cells were fixed with 4 vol % PFA for 5 min at room temperature and then washed three times with PBS for 5 min each. Subsequently, the wells were rinsed thrice with diluted OsteoImage wash. Cells were stained with Alexa 568 phalloidin 1:400 (Molecular Probes) and the cement particles with the OsteoImage staining solution 1:100 (Lonza) for 1 h at room temperature in the dark. After 1 h, the wells were washed three times with the diluted OsteoImage wash for 5 min each and rinsed three times with PBS. Cells were then incubated with NucBlue fixed cell ready probe reagent (Molecular Probes) for 20 min, after which they were rinsed in PBS and mounted using ProLong Diamond antifade reagent (Molecular Probes).

2.7. Cytotoxicity Assay

MC3T3-E1 cells were seeded at 5×10^4 cells/well in a 96-well plate and 2 μL of the cements were added to each well. The cells were incubated with the cements for 48 h in 240 μL of MEM-α without ascorbic acid and with 10 wt %/vol FBS as the culture medium. After 48 h, an MTT assay was performed using the Vybrant MTT Cell Proliferation Assay Kit (Molecular Probes) according to the manufacturer's instructions. All the samples were analyzed in triplicate. The positive control consisted of cells with the growth medium, while the negative control contained only the growth medium without the cells. The absorbance readings for all the samples were normalized with respect to both the negative and the positive control.

2.8. Real-Time qPCR

Total RNA was extracted from RAW264.7 cells incubated with different cement samples using the RNeasy kit (Qiagen). cDNA was synthesized using the High-Capacity cDNA reverse transcription kit (Applied Biosystems) from 100 ng of total RNA and quantified using custom TaqMan probes for cathepsin K (CTSK) Mm00484039_m1, Acp5 (TRAP) Mm00475698_m1, Tnfsf11 (RANKL) Mm00441906_m1 and Polymerase (RNA) II (Polr2a) Mm00839502_m1 on a StepOne Real Time PCR System (Applied Biosystems). The real-time PCR results were analyzed using the $\Delta\Delta C_t$ method and all the data were normalized to the expression levels of Polr2a as the housekeeping gene.

3. RESULTS AND DISCUSSION

3.1. Structural and Morphological Characterization

Figure 1 displays scanning electron micrographs of HAP1 and HAP2 as well as of the self-setting cements obtained using different weight ratios between HAP1 and HAP2. To minimize the particle size effect on the drug release profiles, we attempted to prepare these two precursor powders with as similar of the particle size and shape as possible. As a result, HAP1 and HAP2 particles appeared morphologically indistinguishable from one another based on their respective SEM images (Figure 1a–b). A more detailed analysis, however, demonstrated a lower average particle size and a narrower size distribution for HAP2 compared to HAP1 (Figure 2a,b). Although most particles in both HAP1 and HAP2 were smaller than 100 nm, the majority of HAP2 particles were smaller than 20 nm and there was almost no particles larger than 100 nm, whereas HAP1 particles were found in the broader, 10–250 nm size range. Naturally, a more abrupt precipitation used to make HAP2 resulted in a higher supersaturation and the corresponding nucleation rate, leading to a smaller average particle size than in HAP1, whose reactants were mixed at a lower rate.

HAP is known to follow the aggregational mechanism of growth whereby initially nucleated, ~ 1 nm sized Posner's clusters coalesce to form bigger particles, which may or may not subsequently undergo further aggregation to form even bigger particulate units. One such aggregation was caught in Figure 1c, showing the coalescence of 10–15 nm sized particles into a 100 nm sized one, lying at the high end of HAP2 particle size distribution (Figure 2b). The formation of colloidal particles through aggregation of units primarily nucleated via diffusion is now more of a rule than an exception even outside the biomineralization realm,[25–28] where it has been confirmed on multiple occasions.[29–31] These primary particles are usually amorphous, and their subsequent transition to a crystalline product can be controlled by various biomolecular additives.[32–34] Both HAP1 and HAP2 nanoparticles exhibited a high tendency for aggregation, especially following the admixing of NaH_2PO_4 as the liquid component. This phenomenon is illustrated in Figure 1d–f, where 20–100 nm sized particles are seen forming larger agglomerates with sizes in the micrometer range. Still, that particle singlets only partially undergo aggregation and/or coalescence is seen by comparing particle size distribution histograms obtained from SEM images of precursor HAP1 and HAP2 powders (Figure 2a,b) and of the corresponding cements (Figure 2c–e). While a change in the particle size is negligible during the setting of HAP1 cement, it is more drastic for HAP2. Because of its smaller particle size and higher

reactivity, HAP2 particles undergo coalescence more readily than larger and less reactive HAP1 ones.

X-ray diffractograms of precursor HAP1 and HAP2 powders taken successively in the first 2–3 h from the onset of their isolation as a gelatinous precipitate from the parent solution are shown in Figure 3. Although both powders follow the same transition from the amorphous phase to crystalline HAP, the time scale of this transition differs. Namely, while crystalline HAP appears in HAP1 system 90 min after the beginning of the dehydration process under ambient conditions (Figure 3a), it takes twice more time for crystalline HAP to appear in HAP2 (Figure 3b). This is a direct consequence of the precipitation process: the more abruptly precipitated HAP2, whose particles nucleated at a higher local supersaturation, retained their amorphous character longer than the more slowly precipitated HAP1, whose particles nucleated at a lower local supersaturation. X-ray diffractograms of calcium phosphate cements (1) immediately following the formation, (2) halfway through the setting time, and (3) in the fully set form, are shown in Figure 4. Similar to the precursor powders, the cements in the final, set form all display HAP crystal structure, though with different levels of crystallinity. Thus, HAP2 cements, whose precursor powders took longer to transform to HAP from the initially amorphous precipitate than those comprising HAP1, display a lower crystallinity and a greater percentage of the amorphous phase in the set form than HAP1 cements. This is obvious from comparing the half-width of the diffraction peaks, which broaden as the crystallinity is decreased. The average crystallite size determined using the Scherrer equation applied on the most prominent, (211) diffraction peak at $2\theta = 31.86^\circ$ thus equaled 14.87 nm for HAP1, 12.08 nm for HAP1/HAP2 50/50 and 11.03 nm for HAP2. Clearly, the greater the proportion of HAP2 in the cement, the greater the percentage of the amorphous phase. Figure 4a–c demonstrate that phase transformations occur in the setting cements too, bearing resemblance to those occurring during the formation of the precursor powders. HAP2 cement thus retains its amorphous nature until it initially sets, after which it gradually starts to convert to HAP. On the contrary, the HAP1 cement retains its crystallographic HAP identity throughout the whole setting process. Bone cements containing a mixture of HAP1 and HAP2, though, exhibit a coexisting crystalline and amorphous phase, gradually changing to a dominant crystalline HAP phase halfway through the setting process. We also wanted to check if washing the precipitate with ethanol instead of water would stabilize the amorphous phase in HAP2 by reducing the hydration of the particle surface and minimizing the chances for structural reorganization via the dissolution/reprecipitation mechanism, as it was previously achieved with another HAP.[35] The phase transition to crystalline HAP, however, became accelerated under such conditions, as can be seen by comparing the XRD patterns of semisolidified HAP in Figure 4c,d, suggesting that it predominantly occurs by following a bulk, solid state conversion analogous to the martensitic transformation rather than a dissolution/reprecipitation mechanism. Finally, the formation pathway of the third HAP powder synthesized in this study, HAP3, started also from the amorphous phase, but proceeded through dicalcium phosphate anhydrous, a.k.a. monetite, as an intermediate. As seen from Figure 4e, dehydration at elevated temperatures (80 °C) initiated the transition to HAP. Thus, all the cements, regardless of the formation pathway, form the end product of HAP, the most thermodynamically stable calcium phosphate phase at pH > 4.2.[9,36]

3.2. Setting Time Determination

The bone cement setting times were directly dependent on the weight ratio between the two components: HAP1 and HAP2. As seen from Figure 5a, the greater the content of HAP1 in the cements, the shorter the setting time. In contrast, the greater the content of HAP2, the longer the setting time of the cement. The setting process involves the transition of the amorphous phase into HAP and, logically, the lesser the amount of this active component in the cement, the less time it takes for it to set. This is in agreement with the previous reports on the ability of HAP to act as a seed that speeds up the setting process,[37,38] but in contrast with the studies where lower crystallinity favored dissolution and reprecipitation and accelerated phase transitions of the setting process.[39] The setting time extension effect is equally pronounced for the final and the initial setting time, both of which increase by the factor of 2.4 as the content of HAP1 in the mixed cement decreases from 100 to 0%. Thus, for example, the initial setting time increases from 18 to 21 to 25 to 44 min as the content of HAP1 in the cement decreases from 100 to 85 to 50 to 0%. The final setting time, in turn, changes from 102 min for pure HAP2 to 42 min for pure HAP1. Figure 5b shows the setting time dependence on the weight of the cement. As the weight of the cement decreases, the setting time decreases too, while retaining its characteristic pattern of increasing the setting time with an increase in HAP2 content. As the weight of the cement increases, its surface-to-volume ratio decreases, which entails a lower rate of evaporation of the liquid phase and, thus, a lower setting rate. These rather long setting times could be reduced by decreasing the amount of the liquid, Na_2HPO_4 component in the cements. Longer than therapeutically ideal setting times were employed in this study so as to increase the magnitude of the change of the setting time as a function of the cement composition, an effect that would not be as drastic at shorter setting times.

3.3. In Vitro Drug Release

Similar to the setting reaction, the drug release profiles were also directly dependent on the weight ratio between the two cement components, HAP1 and HAP2. Figure 6a shows the complete time release profiles for vancomycin entrapped within the bone cements. As the weight ratio between the two constituents of the cements, HAP1 and HAP2, is varied, the release patterns drastically change. The least sustained release pattern was seen for pure HAP2, whereas the most sustained one belonged to HAP1, with the two mixed cements falling in-between. The general trend is that the more HAP1 there is in the cement, the more sustained the release of the drug from it, whereas the more HAP2 the cement contains, the more rapid and burst the drug release from it is. Following a short period of burst release, which itself is directly proportional to the content of HAP2 in the cements, ranging from 100% for pure HAP2 to 35% for HAP1/HAP2 50/50 to 18% for pure HAP1, all cements exhibited a subsequent linear, zero-order portion of the release profile extending until the exhaustion at days 0–14 depending on the composition. As seen in Figure 6b, time to complete release follows a linear dependence when plotted against the HAP1/HAP2 weight ratio, allowing for the cement composition to be easily tuned to the desired release time scale. The trend is such that an increase in the amount of HAP1 in the cement extends the drug release, while an increase in the amount of HAP2 exhibits the opposite effect, speeding up the release. The complete release in days, $R_{comp}(x)$, can be represented as a function of the composition x ($1 \geq x \geq 0$), equaling the content of HAP1 in the cement, so that bone

cements entirely formed from HAP1 have $x = 1$, while bone cements entirely formed from HAP2 have $x = 0$:

$$R_{\text{comp}}(x) = Ax - B \quad (1)$$

The constants A and B are 14.1985 and 0.06663, respectively, and the goodness of the fit is confirmed by $R^2 = 0.97787$. Figure 6c shows the burst release profile of vancomycin from the cement as a function of the composition. With an increase in the amount of HAP2 in the cements, the amount of the drug released during this initial burst increases too. The burst release from pure HAP1 is only about 20 wt %, whereas that from pure HAP2 is 100%. HAP1, in that sense, acts as a suppressor of the burst release, which tends to be fostered by HAP2. Finally, Figure 6d demonstrates a drop in the released amount of the drug over time when plotted against different weight ratios of HAP1 and HAP2 in the bone cements. The release of the drug, $R(x, t)$, as a function of the cement composition x and time t in days, can be calculated from eq 2, in which the constants C and D are 1.972 and 0.02351, respectively (Figure 6e,f). The model provides a strong correlation ($R^2 = 0.9245$) between the drug released and the composition and the elapsed time of the cement incubation in PBS. The model provides a succinct means to tailoring the composition of the cement to a desired drug release kinetics.

$$R(x,t) = \left(100 - \frac{Cxe^x}{Dt}\right)\% \quad (2)$$

While HAP1 reacts to gelation with the preserved crystalline structure (Figure 3b), HAP2 transitions back to the amorphous state of its precursor, before returning to HAP structure at the end of the setting process (Figure 4c). The reason for the latter transition presumably lies in the labile apatitic surface layer formed on HAP2 particles during desiccation: the liquid component added at the onset of the cement formation process first triggers the dissolution of this layer and the exposition of the largely amorphous particle core, but as it starts to evaporate, reprecipitation of HAP is initiated and the HAP2 component in the cement restores this apatitic surface. However, a difference between the release profiles of HAP1 and HAP2 cannot stem from their different response to the cement formation process. Instead, because both phases solidify into HAP before the contact with the release solution is made, this difference must be explainable only by a difference in the physicochemical properties of the surface, especially since adsorption is the sole drug loading mechanism in HAP. On the basis of previous reports,[40–42] both the adsorption rate and the desorption rate for most organics tend to reciprocally relate to crystallinity of HAP. If the phase transformation from amorphous to crystalline HAP was driven by the reduction of surface energy,[43] then Gibbs' adsorption isotherm would be able to explain the greater drug adsorption capacity of the amorphous phase, that is, the phase with a higher surface energy as the result of distorted bond lengths and angles, reduced coordination, reduced density due to lattice expansion, larger ionic diffusivity and a larger concentration of surface heterogeneities and defects compared to its crystalline counterpart. However, it is not certain whether gross surface energetics is the main factor driving the adsorption process, especially

because it is known that precipitation of HAP from aqueous solutions, along with that of other biominerals (e.g., calcite[44]), follows the Ostwald–Lussac rule of stages which dictates a successive increase in the interfacial energy of phases[45] as they transform from that of the initial, amorphous precipitate to one or more intermediates to HAP as the final product. Another factor potentially responsible for more extensive drug release is that of solubility. Previously we have shown that the solubility of calcium phosphates is directly proportional to the rate of release of both small organics and large proteins.[46] On that basis, it could be expected that the HAP phase with a greater propensity toward the amorphous state, whose solubility was measured at 2.5×10^{-3} g/L, will release the drug faster than the one settled stably in the form of crystalline HAP, whose solubility was measured at 3×10^{-4} g/L.[47] Because of its greater entropic similarity to the liquid phase from which it is nucleated, amorphous calcium phosphate is also more hydrated than HAP, which contributes to an easier transfer of molecules to and from the surface, facilitating the drug loading and release. On the other hand, hydration of the surface weakens the binding of the proteins[48,49] and an analogous effect may be responsible for the fast desorption of the drug from HAP2 in spite of its intense adsorption. The increased ionic strength as the result of the more pronounced dissolution of HAP2 and the corresponding (a) lowering of the surface charge barrier[50] and (b) increase in surface energy deducible from the Gibbs' isotherm[51] may be another effect that facilitates adsorption and desorption of foreign species, including drug molecules. Finally, a more intense dissolution/reprecipitation activity was earlier detected on an amorphous calcium phosphate particle surface compared to that of HAP,[41] which may be yet another effect favoring the release of surface-bound drug from HAP2 as opposed to HAP1. If only the first few atomic layers of the surface brought into contact with the release solution undergo a similar relapse to the amorphous state as in the case of the cement formation process (Figure 4c), it might cause enough structural disturbances to release the drug from the particle surface. This may explain why the more structurally labile HAP2 does not manage to retain the drug for prolonged periods of time, as opposed to HAP1 whose structural stability is the key to sustained release properties of these two-component, monophasic cements.

Figure 7a displays a comparison between vancomycin release profiles from HAP1 and HAP3. The difference is negligible, suggesting that the alkalinity/acidity of the solution from which HAP is precipitated using the reported method makes insignificant difference in terms of the release profile when these two products are compared alone. However, when they are separately combined with HAP2, a drastic difference in the release profiles is observed (Figure 7b), demonstrating that a synergy between HAP2 and different HAP powders is different and crucially involved in determining the release properties of the resulting cements. Namely, while the 50/50 combination of HAP2 and HAP1 takes 7 or more days for complete release to occur, the burst release for the 50/50 combination of HAP2 and HAP3 completely exhausts the carrier of the drug, making it similar to the release profile of pure HAP2. Also, combining all three HAP powders in equal proportion leads to the completion of the drug release in 2 days, which is three times faster than that observed for the 50/50 combination of HAP1 and HAP2. Although HAP1 and HAP3 per se may perform indistinguishably from one another, the difference between them, interestingly, becomes evident only in combination with HAP2. These findings open the room for the

further exploration of the synergy between different calcium phosphates, regardless of whether their phase composition is identical or dissimilar among each other.

Figure 8a shows the drug release profiles of the cements loaded with a different antibiotic: ciprofloxacin. These kinetic profiles are governed by the same trend as that applying for vancomycin: HAP1 in the cement extends the drug release period, while HAP2 reduces it. Overall, it appears that the longer the powder retains the amorphous nature of the primary precipitate, the more active it is, both in terms of accelerating the setting process and speeding up the release of the adsorbed drug. On the basis of the comparative analysis of the drug release data for vancomycin and ciprofloxacin, it is concluded that the release kinetics does not only depend on the HAP1/HAP2 ratio, but also on the drug. It is widely known that different drugs can have drastically different release profiles from the same carrier[52,53] and that the synergy between the drug and the carrier is the ultimate determinant of the release properties. In this case, the release of ciprofloxacin is more extended for all the cements compared to that of vancomycin. For example, while HAP2 released 100% of vancomycin within the first 24 h (Figure 6a,b), it took 3 days for the same sample to release 100% of ciprofloxacin (Figure 8b). Other cements exhibited a similar behavior. Finally, no visible degradation of the cements paralleled the release process, indicating the release by desorption and diffusion solely and suggesting that degradation in this case does not condition the release of the entrapped drug. A relatively large porosity of the hardened cements, around 50% on average (Table 2), is expected to play a significant role in enabling the release of the drug even in the absence of any visible degradation of the cements. This is seen from the parallel increase in the release rate and the porosity with the amount of HAP2 in the cements (Table 2).

3.4. Antibacterial Tests

The agar diffusion assay for all three bacterial species—*S. aureus, E. coli* and *P. aeruginosa*—showed distinct zones of inhibition around both vancomycinand ciprofloxacin-containing cements after 24 h incubation (Table 3). Markedly more prominent zones of inhibition, however, were observed around all of the ciprofloxacin-containing cements compared to their vancomycin-loaded counterparts. This is a direct consequence of the greater antibacterial potency of ciprofloxacin than that of vancomycin, as evidenced by the larger inhibition zones around pure ciprofloxacin than around pure vancomycin. Vancomycin alone is known to be ineffective against Gram-negative bacterial infections,[54,55] and when assayed against *E. coli* and *P. aeruginosa*, both of which are Gram-negative bacteria, virtually no zone of inhibition formed. In contrast, even pure, vancomycin-free cements showed a zone of inhibition when plated on both *E. coli* and *P. aeruginosa*. The zone of inhibition around vancomycin only was also relatively small when plated against *S. aureus*, but increased for the vancomycin-loaded cements, confirming that the drug and the carrier in this case create a positive synergy rendering it more effective against all three types of bacteria than the pure drug.

Unlike vancomycin, ciprofloxacin demonstrated large zones of bacterial growth inhibition around it against all three types of bacteria. Ciprofloxacin-loaded cements displayed the same trend, with zones of inhibition being large and not varying significantly between

cements. However, the inhibition zones around the ciprofloxacin-loaded cements in agars inoculated with the two Gram-negative bacteria, *E. coli* and *P. aeruginosa*, were larger than those around ciprofloxacin itself, reiterating the aforementioned positive synergy between the antibiotic and the HAP carrier. No such expansion of the inhibition zone was seen when ciprofloxacin-loaded cements were tested against the Gram-positive *S. aureus*.

Interestingly, some of the cements without any vancomycin also showed zones of inhibition, for example, HAP1/HAP2 85/15 and pure HAP2 against *P. aeruginosa* and all four of the antibiotic-free cements against *E. coli*. This further corroborates the idea that cements per se are capable of eliciting an antibacterial response. The first potential cause for this inhibition to consider was the alkaline nature of the cements, given that high pH has been shown to impose stress on Gramnegative bacteria[56] and eradicate them via rapture of cell membrane.[57] However, the pH of the cements was in the mildly alkaline region, equaling 8.5, whereas that of the broths following the overnight incubation with the cements equaled 7.1, implying that alkalinity cannot be the reason for this pronounced antibacterial effect. Another possible reason might be the release of ultrafine cement particles, given that fine particle rings were detected around cements deposited on agar plates. However, the most probable cause of this antibacterial effect is the inherently active surface undergoing phase transformations between the amorphous and the crystalline phase when brought into contact with the agar or the broths. If this is the right mechanism by which bacteria are being annihilated or inhibited in growth, then it might open a whole new avenue in the design of antibacterial surfaces by controlling the incessantly ongoing phase transitions on them.

Liquid broth inoculation tests of vancomycin- and ciprofloxacin- loaded cements and of the corresponding controls against *S. aureus*, *E. coli*, and *P. aeruginosa* (Figures 9 and 10) corroborated the results of the agar diffusion assay and provided a further insight into their ability to act as growth inhibitors. All of the antibiotic-loaded cements exhibited inhibition against all three types of bacteria within the first 2 days. For most of the drug-loaded cements the inhibition increased as the incubation time was extended from 24 to 48 h, indicating a long-term antibacterial effect that is due to the sustained release of the antibiotics. Exceptions to this trend were (a) ciprofloxacin-loaded cements against *E. coli* and *P. aeruginosa* and (b) the combination of the most burst-releasing cement, HAP2, the least effective of the two antibiotics, vancomycin, and the least affected of the three bacterial species, *S. aureus*. Vancomycin itself was moderately effective against *E. coli* and completely ineffective against *P. aeruginosa*, yet all of the four cements loaded with vancomycin exhibited excellent inhibition of both *E. coli* and *P. aeruginosa* in the liquid inoculation assay (Figure 9b,c), reiterating the positive synergy between the carrier and the drug seen in the agar diffusion test too. Ciprofloxacin alone was more effective than vancomycin alone in a sense that, unlike vancomycin, it inhibited all three bacterial species. Loading the cements with ciprofloxacin had the same antibacterial effect as the antibiotic itself (Figure 10b,c). No increase in the effectiveness of the antibiotic delivered together with the cement, observed in the case of vancomycin, was seen for ciprofloxacin, reiterating the importance of the right choice of the carrier and the drug in attempt to provide for the optimal therapeutic synergy of the two.

The majority of the cements not loaded with antibiotics showed growth inhibition, corroborating the results of the agar plate assay. The antibacterial effectiveness of pure cements was, for example, consistently higher than that of pure vancomycin against both types of Gram-negative bacteria: *E. coli* and *P. aeruginosa*. The antibiotic-free cements showed a higher antibacterial activity against the Gram-negative *E. coli* and *P. aeruginosa* (Figures 9b,c and 10b,c) than against the Grampositive *S. aureus* (Figures 9a and 10a), corroborating the results of the agar diffusion assay. This is not to say that pure cements were ineffective against the Gram-positive *S. aureus*. In fact, the concentration of *S. aureus* bacteria in broths decreased in direct proportion with the content of HAP2 in them, being significantly lower compared to the infected but untreated broths for all four compositions after 24 h of incubation (Figures 9a and 10a).

Finally, the antibiofilm assay performed against *P. aeruginosa* biofilms reiterated the finite antibiotic effectiveness of pure, antibiotic-free cements. As seen in Figure 11, all of the pure cements except HAP/HAP2 50/50 significantly decreased the bacterial population in the biofilm following 48 h of incubation. No significant advantage resulted from combining this or any other cement composition with either vancomycin or ciprofloxacin, as in all cases the difference in the antibiotic effect between the antibiotic-loaded cements, the antibiotic-free cements and the antibiotic alone was insignificant. All of them decreased the bacterial population, but none of them fully diminished it, indicating the sturdiness and, as expected, only partial effectiveness of antibiotic therapies of any type against the biofilm structure of *P. aeruginosa*.

3.5. Osteoclastic Interaction and Osteoblastic Viability Assay

Osteoclasts are multinucleated bone cells[58] that play a significant role in the resorption of mineralized tissues during bone remodeling.[59] Osteoclast-induced bone resorption, in fact, precedes osteoblast-induced bone formation during this process.[60] Also, disrupted resorptive activity of the osteoclasts can lead to bone diseases such as osteoporosis,[61] osteoarthritis,[62] and malignant metastases of bone.[63] Therefore, to achieve proper bone regeneration, it is of primary importance for the bone implant to induce a healthy interaction not only with osteoblasts, but also with osteoclasts.

In this in vitro biocompatibility test, the response of osteoclastic RAW264.7 cells to the self-setting bone cements was followed using fluorescent optical microscopy. TRAP staining confirmed the osteoclastic, multinucleated morphology of differentiated RAW264.7 cells incubated with the cements, while the upregulation of the osteoclastic markers TRAP and CTSK, as well as the negligible expression of the osteoblastic markers Runx2 and RANKL, were detected in a subsequent qPCR analysis, demonstrating that the RAW264.7 cells did correctly differentiate into osteoclasts (Figure 12f). In addition to the detection of multiple nuclei inside the cells, the morphological analysis of the cells further evidenced the presence of a ruffled border with villi-like cytoskeletal structures (Figure 12a), which is a characteristic feature of osteoclasts engaged in bone resorption.[64] No morphological defects were observed in the osteoclasts during the uptake of the cements. As can be seen in Figure 12b–e, a large amount of cement particles was being internalized by the cells after 9 days of incubation, a reliable indicator of the biocompatibility and resorbability of the bone cements.

As far as the interaction with osteoblasts was concerned, the cell viability of the osteoblastic MC3T3-E1 cell line in the presence of the cements decreased in direct proportion with the content of HAP2 in them. The same effect was also observed against *S. aureus* in broths, confirming the high activity of HAP2 phase. Still, this decrease in viability was statistically significant only for the pure HAP2 cement (Figure 13). Statistically insignificant decrease in cell viability was detected for the three other cement compositions, suggesting the overall good biocompatibility of the cements with the osteoblastic cells. All in all, in spite of their exhibiting a moderate antibacterial effect on some bacterial populations even without being loaded with the antibiotics, no adverse effects on bone cells were observed. Such selective behavior, osteophilic yet antimicrobial, is rarely observed, given that most antibacterial materials and surfaces hinder the attachment of bone cells, whereas those that promote bone integration are usually prone to biofilm adhesion.[65]

4. SUMMARY

Self-setting calcium phosphate cement formulations have opened up a new avenue in the development of advanced bone regeneration implants.[66,47,67] They have allowed for the design of injectable, precisely localizable grafts adaptable to the geometry of the bone defect and applicable in minimally invasive orthopedic and craniofacial surgery. Like most self-setting calcium phosphate cements, the one developed in this study had two primary components: a solid powder, which was a combination of different types of hydroxyapatite, and a liquid component, which acts as a hardener and helps in setting the cement. In general, the mixing of the solid powder and the aqueous component induces chemical transformations of one calcium phosphate phase to another, and either brushite or HAP is the final phase, the latter of which sets slower and is mechanically superior to the former.[67] The formation pathways, setting and drug release properties, antibacterial behavior, and cell compatibility of the cements setting into HAP as the final phase have been explored in this study. We used two different HAP powders as components of the solid phase, differing in the abruptness of the precipitation process and in the duration of the preservation of the amorphous phase before it eventually transforms into crystalline HAP. The phases maintaining their amorphous nature for shorter and longer periods of time were termed HAP1 and HAP2, respectively. The weight ratio between these two components in the cement determined its setting rate and the drug release kinetics for two different antibiotics, vancomycin and ciprofloxacin. The greater the content of HAP1 in the cement, the faster the setting and the slower the release. In contrast, the greater the content of HAP2 in the cement, the slower the setting and the faster the release. The drug release profiles could be predicted and easily tuned to the desired properties using a set of equations empirically derived to fit the experimental release patterns.

Because of a lesser potential to control the structural parameters in a tunable manner and because of a lesser drug entrapment capacity, inorganic systems have been more challenging to use as carriers in controlled drug delivery than the polymers. Still, different inorganic powder properties have been previously modified in an attempt to control the drug release kinetics, though mostly in a robust, unsystematic way, allowing for no truly tunable controlled release to be achieved. These intrinsic parameters have included the powder composition,[46] particle size,[68] crystallinity,[69] porosity,[70–72] concentration of dopants,[73]

polymorphic transitions,[74] particle shell-to-core volume ratio,[75] rotation speed of nanoparticles in a nanomotor,[76] and so on. In this study, we demonstrate for the first time that the kinetics of the mechanism of formation of a solid compound can be controlled to produce tunable and numerically fittable drug release profiles. More specifically, by varying the content of the self-setting CAP cements between that of pure HAP2 on one extreme and that of pure HAP1 on the other extreme, the drug release time scales were varied between zero and 15 days. The setting times were also made tunable using the same principle, and the only difference was that other parameters, including the weight of the cements, affected them as well. One of the broad connotations of this study is the demonstration that the history of the formation of a material structure can sometimes be a more important determinant of its properties than this structure per se.

The antibiotic-loaded cement formulations were highly effective against both Gram-positive bacteria such as *S. aureus* and Gram-negative ones such as *E. coli* and *P. aeruginosa*. However, even the pure cements exhibited an antibacterial effect ranging from moderate to strong, albeit demonstrating high levels of compatibility with both osteoclastic and osteoblastic bone cells. This antimicrobial effect was especially noticeable against Gram-negative bacteria, where the growth inhibition by the cements was comparable to or, at times, even stronger than that of the pure antibiotics. At other times, the cement carriers provided an additive effect by increasing the antibacterial effectiveness of the pure antibiotic. We suspect that the antibacterial activity of the surface of the particles comprising the cements is owing to the phase transitions to and from the amorphous and crystalline HAP phases. However, exploring the phase transitions, surface transformations, and ultrafine particle release that take place in the course of the interaction of the cements with bacteria and that might be responsible for eliciting this antibacterial effect will be the subject of continued studies. The flexibility intrinsic to the cements, both in terms of drug loading, drug release, and setting characteristics, enabling their use as carriers and grafts tunable to the therapeutic occasion, is the key to their exciting applicative potential in orthopedic and dental clinics. It is also another line on the already long list of versatile properties of calcium phosphates and further proof of fascinating yet still largely unexplored physicochemical proteanism exhibited by this material, of which the physical foundations of our bodies are being made.

Acknowledgments

The authors acknowledge the National Institutes of Health grant R00-DE021416 for support. SEM imaging was conducted at the Research Resources Center of the UIC.

REFERENCES

1. Uskoković V. Nanostructured Platforms for the Sustained and Local Delivery of Antibiotics in the Treatment of Osteomyelitis. Crit. Rev. Ther. Drug Carrier Syst. 2015; 32:1–59. [PubMed: 25746204]
2. Spellberg B, Lipsky BA. Systemic Antibiotic Therapy for Chronic Osteomyelitis in Adults. Clin. Infect. Dis. 2012; 54:393–407. [PubMed: 22157324]
3. Sabtu N, Enoch DA, Brown NM. Antibiotic Resistance: What, Why, Where, When and How? Br. Med. Bull. 2015; 116:105–113. [PubMed: 26491083]

4. Obalum DC, Nzewi C, Fiberesima F, Onubi OJ. Chronic Recurrent Multifocal Osteomyelitis: A Case Report and Review of Literature. West Afr. J. Med. 2013; 30:453–456. [PubMed: 22786864]
5. Rao N, Ziran BH, Lipsky BA. Treating Osteomyelitis: Antibiotics and Surgery. Plast. Reconstr. Surg. 2011; 127:177S–187S. [PubMed: 21200289]
6. Theologie-Lygidakis N, Schoinohoriti O, Iatrou I. Surgical Management of Primary Chronic Osteomyelitis of the Jaws in Children: A Prospective Analysis of Five Cases and Review of the Literature. Oral Maxillofac. Surg. 2011; 15:41–50. [PubMed: 20978813]
7. Ginebra M-P, Traykova T, Planell JA. Calcium Phosphate Cements as Bone Drug Delivery Systems: A Review. J. Controlled Release. 2006; 113:102–110.
8. Verron E, Khairoun I, Guicheux J, Bouler J-M. Calcium Phosphate Biomaterials as Bone Drug Delivery Systems: A Review. Drug Discovery Today. 2010; 15:547–552. [PubMed: 20546919]
9. Ginebra M-P, Canal C, Espanol M, Pastorino D, Montufar EB. Calcium Phosphate Cements as Drug Delivery Materials. Adv. Drug Delivery Rev. 2012; 64:1090–1110.
10. Kibalczyc W, Zielenkiewicz A, Zielenkiewicz W. Calorimetric Investigations of Calcium Phosphate Precipitation in Relation to Solution Composition and Temperature. Thermochim. Acta. 1988; 131:47–55.
11. Otsuka M, Matsuda Y, Suwa Y, Fox JL, Higuchi WI. Effect of Particle Size of Metastable Calcium Phosphates on Mechanical Strength of a Novel Self-setting Bioactive Calcium Phosphate Cement. J. Biomed. Mater. Res. 1995; 29:25–32. [PubMed: 7713955]
12. Barralet JE, Grover LM, Gbureck U. Ionic Modification of Calcium Phosphate Cement Viscosity. Part II: Hypodermic Injection and Strength Improvement of Brushite Cement. Biomaterials. 2004; 25:2197–2203. [PubMed: 14741635]
13. Bohner M, Van Landuyt P, Merkle HP, Lemaitre J. Composition Effects on the pH of a Hydraulic Calcium Phosphate Cement. J. Mater. Sci.: Mater. Med. 1997; 8:675–681. [PubMed: 15348818]
14. Ginebra MP, Fernandez E, Driessens FCM, Boltong MG, Muntasell J, Font J, Planell JA. The Effects of Temperature on the Behaviour of an Apatitic Calcium Phosphate Cement. J. Mater. Sci.: Mater. Med. 1995; 6:857–860.
15. Lee, DD.; Rey, C.; Aiolova, M.; Tofighi, A. Method of Preparing a Poorly Crystalline Calcium Phosphate and Methods of Its Use. U.S. Patent No. 6953594. 2005 Oct 11.
16. Meier, DE.; Rouma, BS. Haematogenous Osteomyelitis and Septic Arthritis. In: Ameh, EA.; Bickler, SW.; Lakhoo, K.; Nwomeh, BC.; Poenaru, D., editors. Paediatric Surgery: A Comprehensive Text for Africa. Vol. 6. Seattle: Global HELP Organization; 2011. p. 135-140.
17. Baldan M, Gosselin RA, Osman Z, Barrand KG. Chronic Osteomyelitis Management in Austere Environments: The International Committee of the Red Cross Experience. Trop. Med. Int. Health. 2014; 19:832–837. [PubMed: 24702780]
18. Desai TA, Uskoković V. Calcium Phosphate Nanoparticles: A Future Therapeutic Platform for the Treatment of Osteomyelitis? Ther. Delivery. 2013; 4:643.
19. Felix Lanao RP, Leeuwenburgh SCG, Wolke JGC, Jansen JA. Bone Response to Fast-Degrading, Injectable Calcium Phosphate Cements Containing PLGA Microparticles. Biomaterials. 2011; 32:8839–8847. [PubMed: 21871661]
20. Burguera EF, Xu HHK, Sun L. Injectable Calcium Phosphate Cement: Effects of Powder-to-liquid Ratio and Needle Size. J. Biomed. Mater. Res., Part B. 2008; 84:493–502.
21. Sun L, Chow LC, Frukhtbeyn SA, Bonevich JE. Preparation and Properties of Nanoparticles of Calcium Phosphates with Various Ca/P Ratios. J. Res. Natl. Inst. Stand. Technol. 2010; 115:243. [PubMed: 21037948]
22. Elliott JC. Structure and Chemistry of the Apatites and Other Calcium Orthophosphates. Stud. Inorg. Chem. 1994; 18:1–389.
23. Dental Zinc Phosphate Cement. Geneva, Switzerland: ISO 1566International Organization for Standardization; 1978.
24. Xue B, Zhang C, Wang Y, Wang J, Zhang J, Lu M, Li G, Cao Z, Huang Q. A Novel Controlled-Release System for Antibacterial Enzyme Lysostaphin Delivery Using Hydroxyapatite/Chitosan Composite Bone Cement. PLoS One. 2014; 9:e113797. [PubMed: 25464506]
25. Meldrum FC, Sear RP. Now You See Them. Science. 2008; 322:1802–1803. [PubMed: 19095931]

26. Hu Q, Nielsen MH, Freeman CL, Hamm LM, Tao J, Lee JRI, Han TY-J, Becker U, Harding JH, Dove PM. The Thermodynamics of Calcite Nucleation at Organic Interfaces: Classical vs. Non-Classical Pathways. Faraday Discuss. 2012; 159:509–523.
27. Matijević E. Nanosize Precursors as Building Blocks for Monodispersed Colloids. Colloid J. 2007; 69:29–38.
28. Anand U, Lu J, Loh D, Aabdin Z, Mirsaidov U. Hydration Layer-Mediated Pairwise Interaction of Nanoparticles. Nano Lett. 2015; 16:786–790. [PubMed: 26709603]
29. Dey A, Bomans PHH, Müller FA, Will J, Frederik PM, de With G, Sommerdijk NAJM. The Role of Prenucleation Clusters in Surface-Induced Calcium Phosphate Crystallization. Nat. Mater. 2010; 9:1010–1014. [PubMed: 21076415]
30. Pouget EM, Bomans PHH, Goos JACM, Frederik PM, Sommerdijk NAJM, de With G. The Initial Stages of Template-Controlled CaCO3 Formation Revealed by Cryo-TEM. Science. 2009; 323:1455–1458. [PubMed: 19286549]
31. Mahamid J, Addadi L, Weiner S. Crystallization Pathways in Bone. Cells Tissues Organs. 2011; 194:92–97. [PubMed: 21576906]
32. Gajjeraman S, Narayanan K, Hao J, Qin C, George A. Matrix Macromolecules in Hard Tissues Control the Nucleation and Hierarchical Assembly of Hydroxyapatite. J. Biol. Chem. 2007; 282:1193–1204. [PubMed: 17052984]
33. Kwak S-Y, Kim S, Yamakoshi Y, Simmer JP, Beniash E, Margolis HC. Regulation of Calcium Phosphate Formation by Native Amelogenins in Vitro. Connect. Tissue. Res. 2014; 55:S21–S24.
34. Tao J, Pan H, Zeng Y, Xu X, Tang R. Roles of Amorphous Calcium Phosphate and Biological Additives in the Assembly of Hydroxyapatite Nanoparticles. J. Phys. Chem. B. 2007; 111:13410–13418. [PubMed: 17979266]
35. Boskey AL, Posner AS. Conversion of Amorphous Calcium Phosphate to Microcrystalline Hydroxyapatite. A pH-Dependent, Solution-Mediated, Solid-Solid Conversion. J. Phys. Chem. 1973; 77:2313–2317.
36. Chow LC. Next Generation Calcium Phosphate-Based Biomaterials. Dent. Mater. J. 2009; 28:1–10. [PubMed: 19280963]
37. Ginebra MP, Driessens FCM, Planell JA. Effect of the Particle Size on the Micro and Nanostructural Features of a Calcium Phosphate Cement: A Kinetic Analysis. Biomaterials. 2004; 25:3453–3462. [PubMed: 15020119]
38. Bohner M, Brunner TJ, Stark WJ. Controlling the Reactivity of Calcium Phosphate Cements. J. Mater. Chem. 2008; 18:5669–5675.
39. Bohner M. Reactivity of Calcium Phosphate Cements. J. Mater. Chem. 2007; 17:3980–3986.
40. Uskoković V, Desai TA. Phase Composition Control of Calcium Phosphate Nanoparticles for Tunable Drug Delivery Kinetics and Treatment of Osteomyelitis. II. Antibacterial and Osteoblastic Response. J. Biomed. Mater. Res., Part A. 2013; 101:1427–1436.
41. Lee W, Zavgorodniy AV, Loo C, Rohanizadeh R. Synthesis and Characterization of Hydroxyapatite with Different Crystallinity: Effects on Protein Adsorption and Release. J. Biomed. Mater. Res., Part A. 2012; 100:1539–1549.
42. Ouizat S, Barroug A, Legrouri A, Rey C. Adsorption of Bovine Serum Albumin on Poorly Crystalline Apatite: Influence of Maturation. Mater. Res. Bull. 1999; 34:2279–2289.
43. Mossaad C, Tan M-C, Starr M, Payzant EA, Howe JY, Riman RE. Size-Dependent Crystalline to Amorphous Uphill Phase Transformation of Hydroxyapatite Nanoparticles. Cryst. Growth Des. 2011; 11:45–52.
44. Rodriguez-Blanco JD, Shaw S, Benning LG. The Kinetics and Mechanisms of Amorphous Calcium Carbonate (ACC) Crystallization to Calcite, via Vaterite. Nanoscale. 2011; 3:265–271. [PubMed: 21069231]
45. Nancollas GH, Wu W. Biomineralization Mechanisms: A Kinetics and Interfacial Energy Approach. J. Cryst. Growth. 2000; 211:137–142.
46. Uskoković V, Desai TA. Phase Composition Control of Calcium Phosphate Nanoparticles for Tunable Drug Delivery Kinetics and Treatment of Osteomyelitis. I. Preparation and Drug Release. J. Biomed. Mater. Res., Part A. 2013; 101:1416–1426.

47. Dorozhkin SV. Self-Setting Calcium Orthophosphate Formulations. J. Funct. Biomater. 2013; 4:209–311. [PubMed: 24956191]
48. Hanein D, Geiger B, Addadi L. Fibronectin Adsorption to Surfaces of Hydrated Crystals. An Analysis of the Importance of Bound Water in Protein-Substrate Interactions. Langmuir. 1993; 9:1058–1065.
49. Flade K, Lau C, Mertig M, Pompe W. Osteocalcin-Controlled Dissolution-Reprecipitation of Calcium Phosphate under Biomimetic Conditions. Chem. Mater. 2001; 13:3596–3602.
50. Uskoković V. Dynamic Light Scattering Based Micro-electrophoresis: Main Prospects and Limitations. J. Dispersion Sci. Technol. 2012; 33:1762–1786.
51. Chattoraj DK, Birdi KS. Spread Monolayer BT - Adsorption and the Gibbs Surface Excess. Adsorption and the Gibbs Surface Excess. 1984:179–232.
52. Liu P, Krishnan TR. Alginate-Pectin-Poly-L-lysine Particulate as a Potential Controlled Release Formulation. J. Pharm. Pharmacol. 1999; 51:141–149. [PubMed: 10217312]
53. Ogomi D, Serizawa T, Akashi M. Controlled Release Based on the Dissolution of a Calcium Carbonate Layer Deposited on Hydrogels. J. Controlled Release. 2005; 103:315–323.
54. French GL. Enterococci and Vancomycin Resistance. Clin. Infect. Dis. 1998; 27:S75–S83. [PubMed: 9710674]
55. van Houten MA, Uiterwaal CSPM, Heesen GJM, Arends JP, Kimpen JLL. Does the Empiric Use of Vancomycin in Pediatrics Increase the Risk for Gram-Negative Bacteremia? Pediatr. Infect. Dis. J. 2001; 20:171–177. [PubMed: 11224837]
56. Padan E, Bibi E, Ito M, Krulwich TA. No Title. Biochim. Biophys. Acta, Biomembr. 2005; 1717:67–88.
57. Mendonca AF, Amoroso TL, Knabel SJ. Destruction of Gram-Negative Food-Borne Pathogens by High pH Involves Disruption of the Cytoplasmic Membrane. Appl. Environ. Microbiol. 1994; 60:4009–4014. [PubMed: 7993089]
58. Okazaki Y, Abe Y, Yasuda K, Hiasa K, Hirata I. Osteoclast Response to Bioactive Surface Modification of Hydroxyapatite. Open J. Stomatol. 2014; 4:340–344.
59. Maria SM, Prukner C, Sheikh Z, Müller FA, Komarova SV, Barralet JE. Characterization of Biomimetic Calcium Phosphate Labeled with Fluorescent Dextran for Quantification of Osteoclastic Activity. Acta Biomater. 2015; 20:140–146. [PubMed: 25829107]
60. Seeman E, Delmas PD. Bone Quality—the Material and Structural Basis of Bone Strength and Fragility. N. Engl. J. Med. 2006; 354:2250–2261. [PubMed: 16723616]
61. Hughes DE, Dai A, Tiffee JC, Li HH, Mundy GR, Boyce BF. Estrogen Promotes Apoptosis of Murine Osteoclasts Mediated by TGF–β. Nat. Med. 1996; 2:1132–1136. [PubMed: 8837613]
62. Durand M, Komarova SV, Bhargava A, Trebec-Reynolds DP, Li K, Fiorino C, Maria O, Nabavi N, Manolson MF, Harrison RE, et al. Monocytes from Patients with Osteoarthritis Display Increased Osteoclastogenesis and Bone Resorption: The In Vitro Osteoclast Differentiation in Arthritis Study. Arthritis Rheum. 2013; 65:148–158. [PubMed: 23044761]
63. Halvorson KG, Sevcik MA, Ghilardi JR, Rosol TJ, Mantyh PW. Similarities and Differences in Tumor Growth, Skeletal Remodeling and Pain in an Osteolytic and Osteoblastic Model of Bone Cancer. Clin. J. Pain. 2006; 22:587–600. [PubMed: 16926574]
64. Vaananen HK, Zhao H, Mulari M, Halleen JM. The Cell Biology of Osteoclast Function. J. Cell. Sci. 2000; 113:377–381. [PubMed: 10639325]
65. Graham MV, Mosier AP, Kiehl TR, Kaloyeros AE, Cady NC. Development of Antifouling Surfaces to Reduce Bacterial Attachment. Soft Matter. 2013; 9:6235–6244.
66. Loca D, Sokolova M, Locs J, Smirnova A, Irbe Z. Calcium Phosphate Bone Cements for Local Vancomycin Delivery. Mater. Sci. Eng., C. 2015; 49:106–113.
67. Dorozhkin SV. Self-Setting Calcium Orthophosphate Formulations: Cements, Concretes, Pastes and Putties. Int. J. Mater. Chem. 2011; 1:1–48.
68. Zhang P, Gómez De La Torre TZ, Forsgren J, Bergström C, Strømme M. Diffusion-Controlled Drug Release from the Mesoporous Magnesium Carbonate Upsalite. J. Pharm. Sci. 2016 in press, doi: 10565766310.1002/jps.24553.

69. Hamanishi C, Kitamoto K, Tanaka S, Otsuka M, Kitahashi T, Doi Y. A Self-setting TTCP-DCPD Apatite Cement for Release of Vancomycin. J. Biomed. Mater. Res. 1996; 33:139–143. [PubMed: 8864885]

70. Pastor EL, Reguera-Nuñez E, Matveeva E, Garcia-Fuentes M. Pore Size Is a Critical Parameter for Obtaining Sustained Protein Release from Electrochemically Synthesized Mesoporous Silicon Microparticles. PeerJ. 2015; 3:e1277. [PubMed: 26557423]

71. Hou H, Nieto A, Ma F, Freeman WR, Sailor MJ, Cheng L. Tunable Sustained Intravitreal Drug Delivery System for Daunorubicin Using Oxidized Porous Silicon. J. Controlled Release. 2014; 178:46–54.

72. Martinez JO, Chiappini C, Ziemys A, Faust AM, Kojic M, Liu X, Ferrari M, Tasciotti E. Engineering Multi-Stage Nanovectors for Controlled Degradation and Tunable Release Kinetics. Biomaterials. 2013; 34:8469–8477. [PubMed: 23911070]

73. Lu D, Lei J, Wang L, Zhang J. Multifluorescently Traceable Nanoparticle by a Single-Wavelength Excitation with Color-Related Drug Release Performance. J. Am. Chem. Soc. 2012; 134:8746–8749. [PubMed: 22591275]

74. Sergeeva A, Sergeev R, Lengert E, Zakharevich A, Parakhonskiy B, Gorin D, Sergeev S, Volodkin D. Composite Magnetite and Protein Containing CaCO3 Crystals. External Manipulation and Vaterite→ Calcite Recrystallization-Mediated Release Performance. ACS Appl. Mater. Interfaces. 2015; 7:21315–21325. [PubMed: 26348458]

75. Orellana BR, Puleo DA. Tailored Sequential Drug Release from Bilayered Calcium Sulfate Composites. Mater. Sci. Eng., C. 2014; 43:243–252.

76. Xu X, Kim K, Fan D. Tunable Release of Multiplex Biochemicals by Plasmonically Active Rotary Nanomotors. Angew. Chem., Int. Ed. 2015; 54:2525–2529.

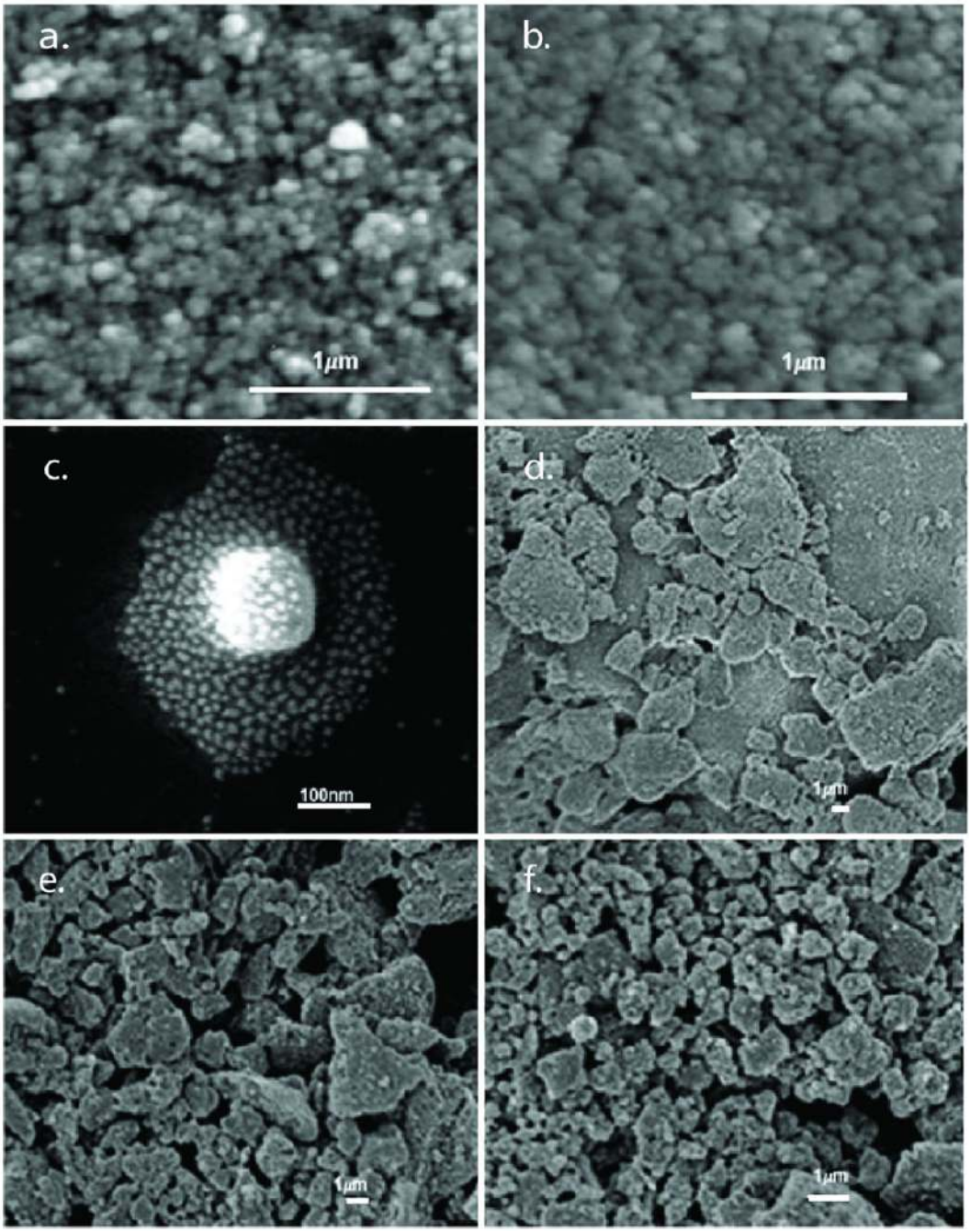

Figure 1.
Scanning electron micrographs of (a) HAP1 and (b) HAP2 nanoparticles formed by (c) aggregation of smaller nanosized units and comprising the precursor powders used to make the cements composed of (d) HAP1 only, (e) HAP2 only, and (f) a 50/50 combination of HAP1 and HAP2.

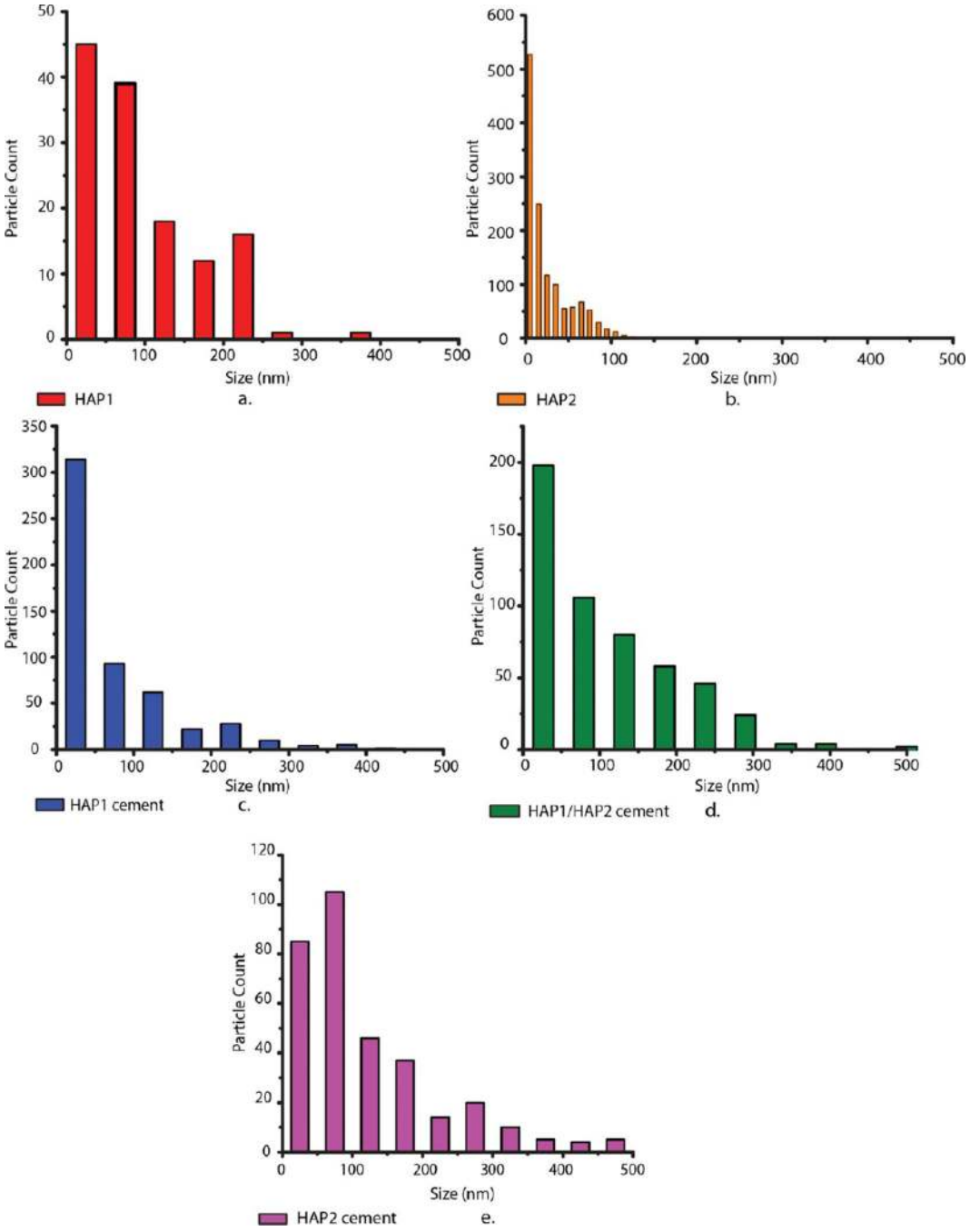

Figure 2.

Particle size distribution histograms for (a) HAP1 and (b) HAP2 precursor powders and for the cements comprising them: (c) HAP1, (d) HAP1/HAP2 50/50, and (e) HAP2.

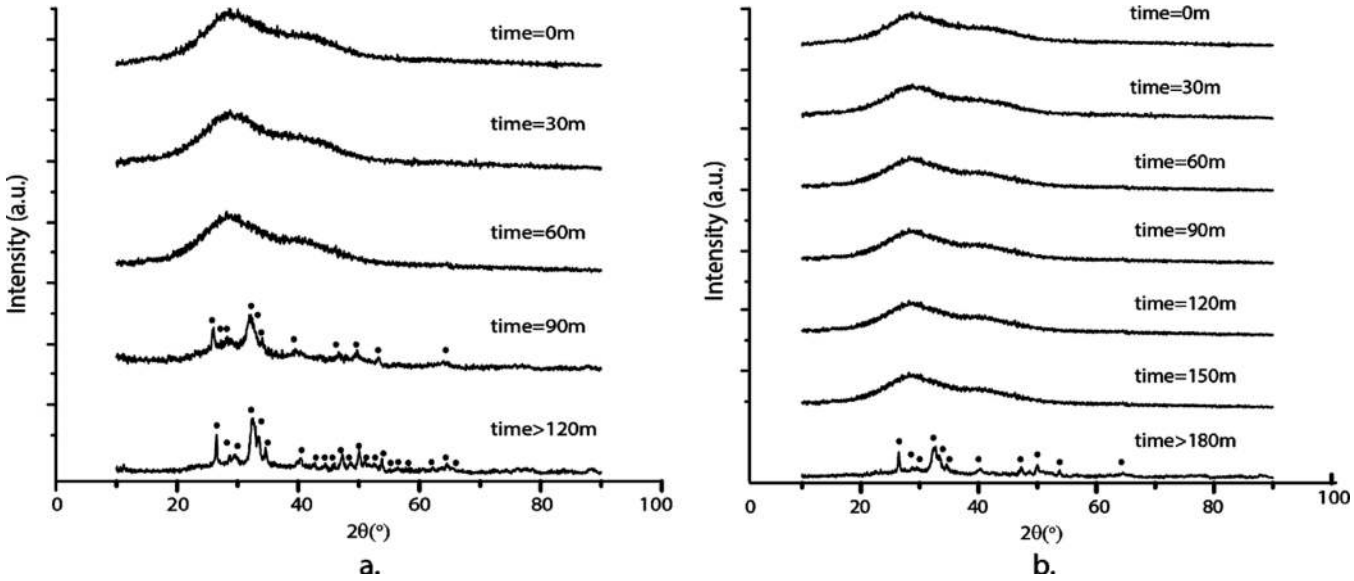

Figure 3.

XRD patterns of (a) HAP1 and (b) HAP2 powders taken at each 30 min from the moment of separation of the precipitate from the parent solution to the end of the following (a) 2 or (b) 3 hours. Diffraction peaks originating from HAP are indexed with ●.

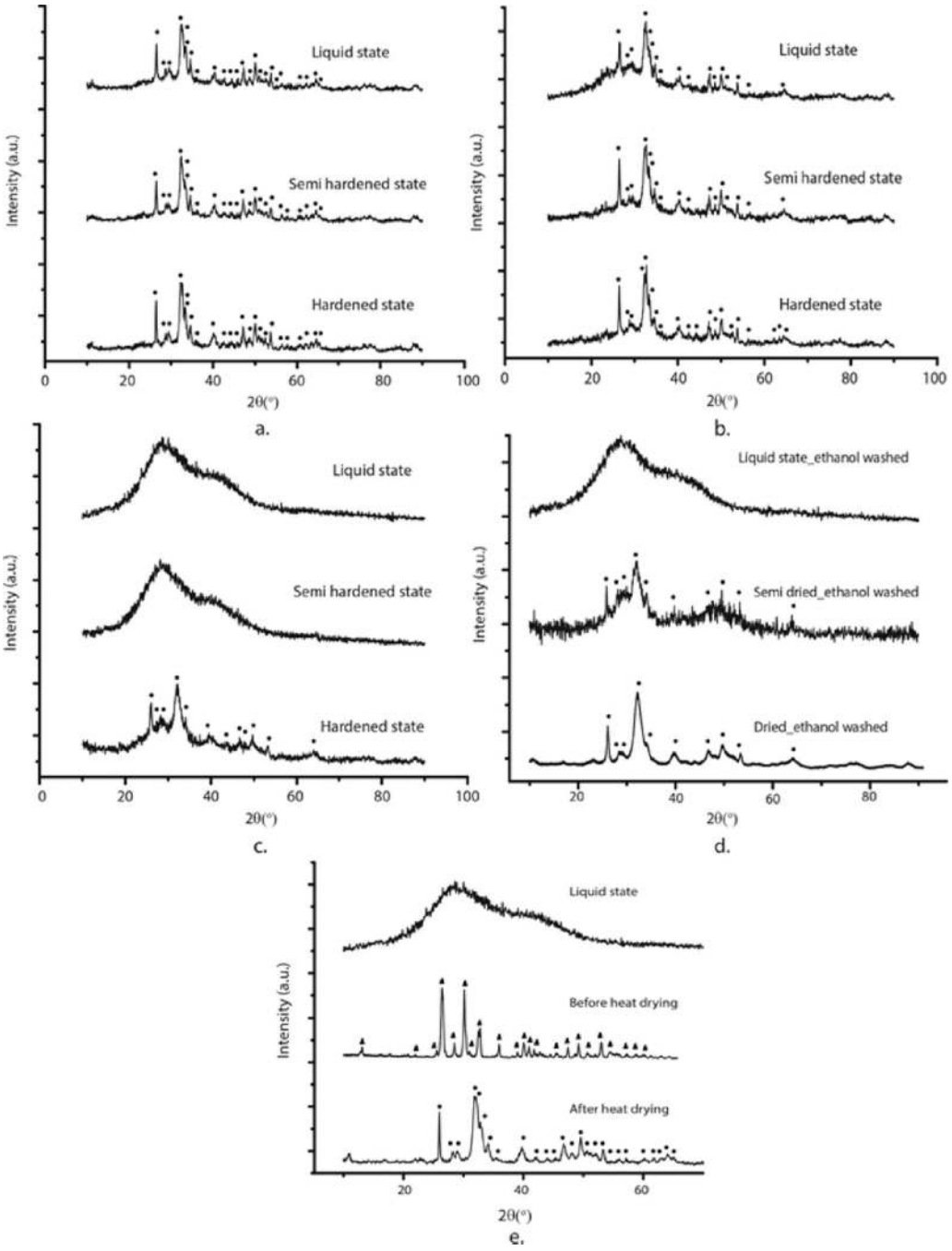

Figure 4.

XRD patterns of HAP1 (a), HAP1/HAP2 50/50 (b) and HAP2 (c) cements as they change their physical state from liquid to solid during the setting process. (d) XRD patterns of HAP2 precursor powder washed with ethanol, not water, as it transforms from liquid to semidried to dried state. (e) XRD patterns of HAP3 powder before and after heat drying, demonstrating the presence of monetite as the intermediate phase. Diffraction peaks originating from HAP are indexed with ●, whereas those originating from monetite are indexed with▲.

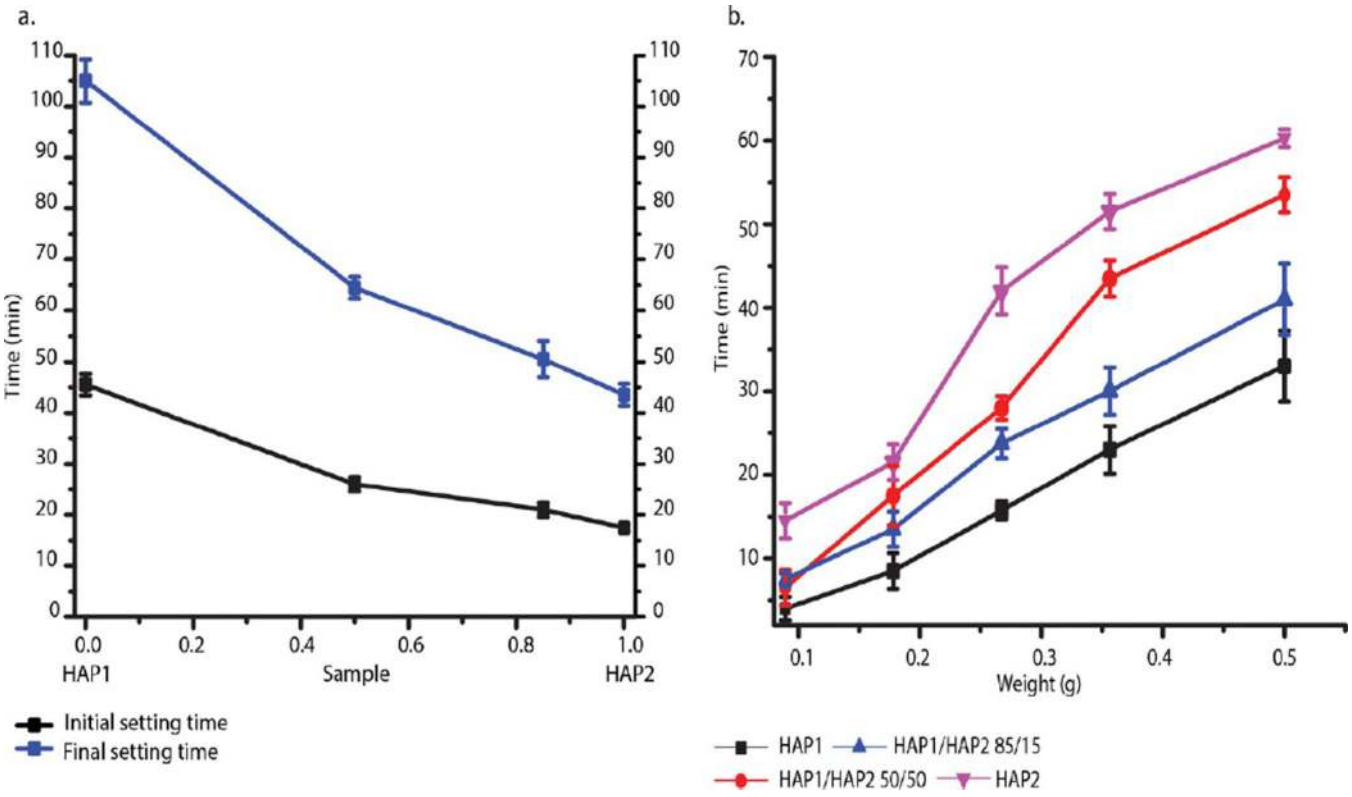

Figure 5.

(a) Initial and final setting times of the self-setting bone cements as a function of the HAP1/HAP2 weight ratio. (b) Dependence of the setting times on the weight of the bone cements analyzed. Data are shown as averages, and error bars represent standard deviation.

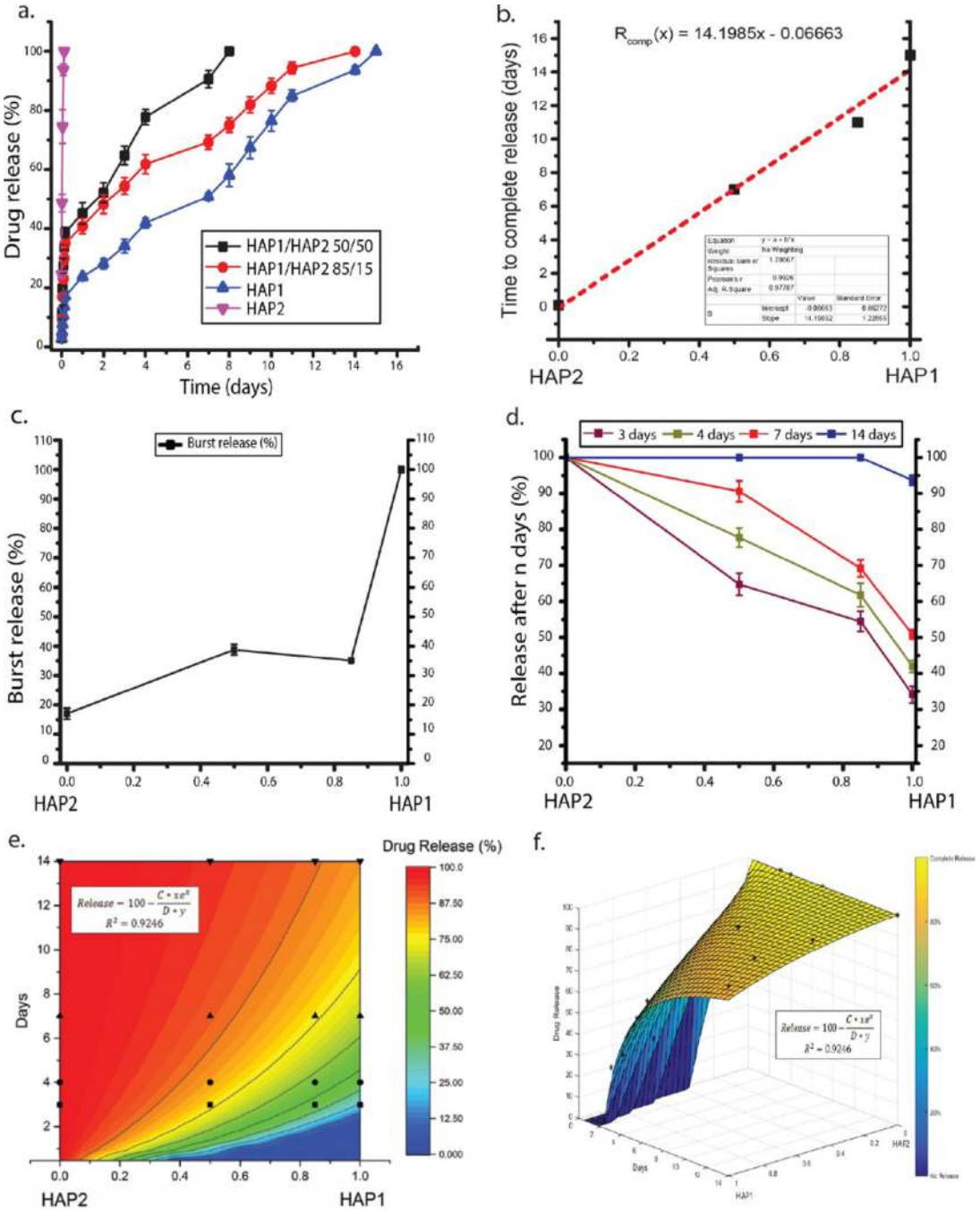

Figure 6.

(a) Vancomycin release profiles of cements composed of HAP1 and HAP2 alone and HAP1 and HAP2 admixed in 85/15 and 50/50 weight ratios. (b) Time to complete release of vancomycin from the same four types of cements in panel a. (c) Burst release profiles for the same four types of cements as in panel a. (d) Vancomycin release after specific periods of time (days in this case) for the same four types of cements as in panel a, along with the three-dimensional (e) and the two-dimensional (f) drug release contours derived from the two-variable in vitro release model, where the composition of the bone cement and the days

elapsed determine the drug release in percentages. Data are shown as averages, and error bars represent standard deviation.

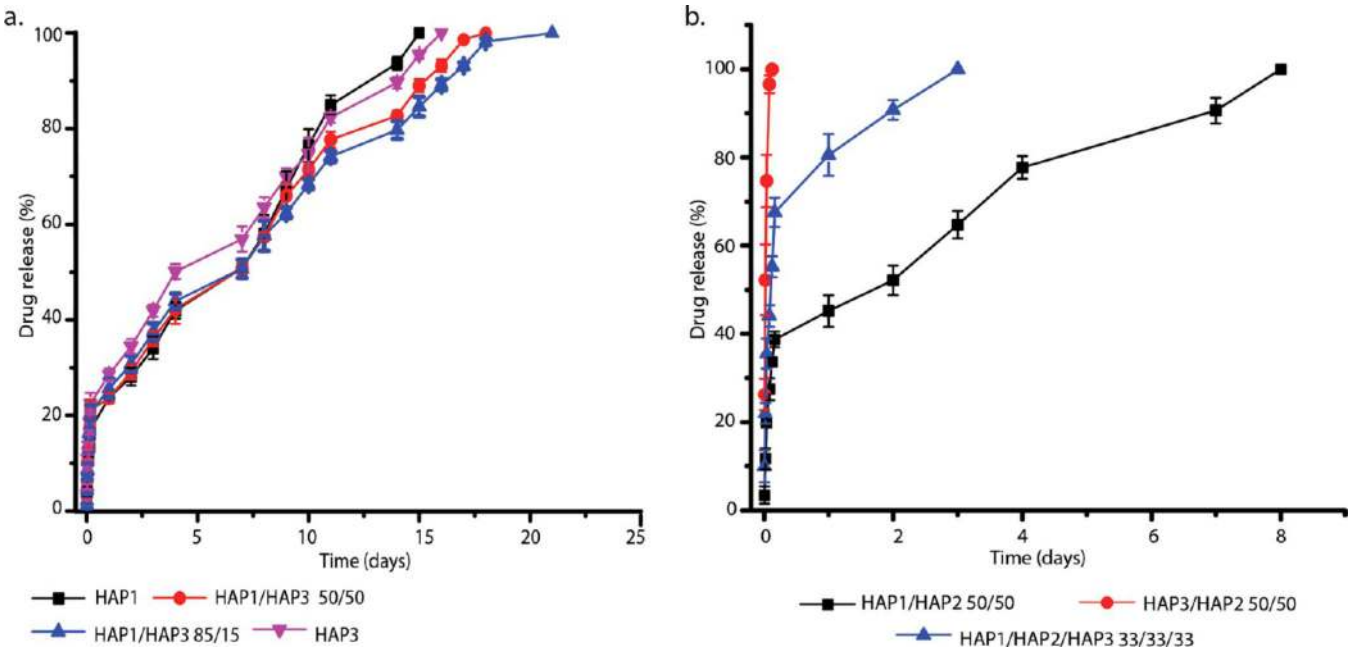

Figure 7.

(a) Comparative vancomycin release profiles for HAP1 and HAP3, indicating the similarity of their release kinetics when compared alone. (b) Comparative vancomycin release profiles for HAP1 and HAP3 in the presence of HAP2, showing how drastically changed their release behavior becomes when they are combined with HAP2. Data are shown as averages with error bars representing standard deviation.

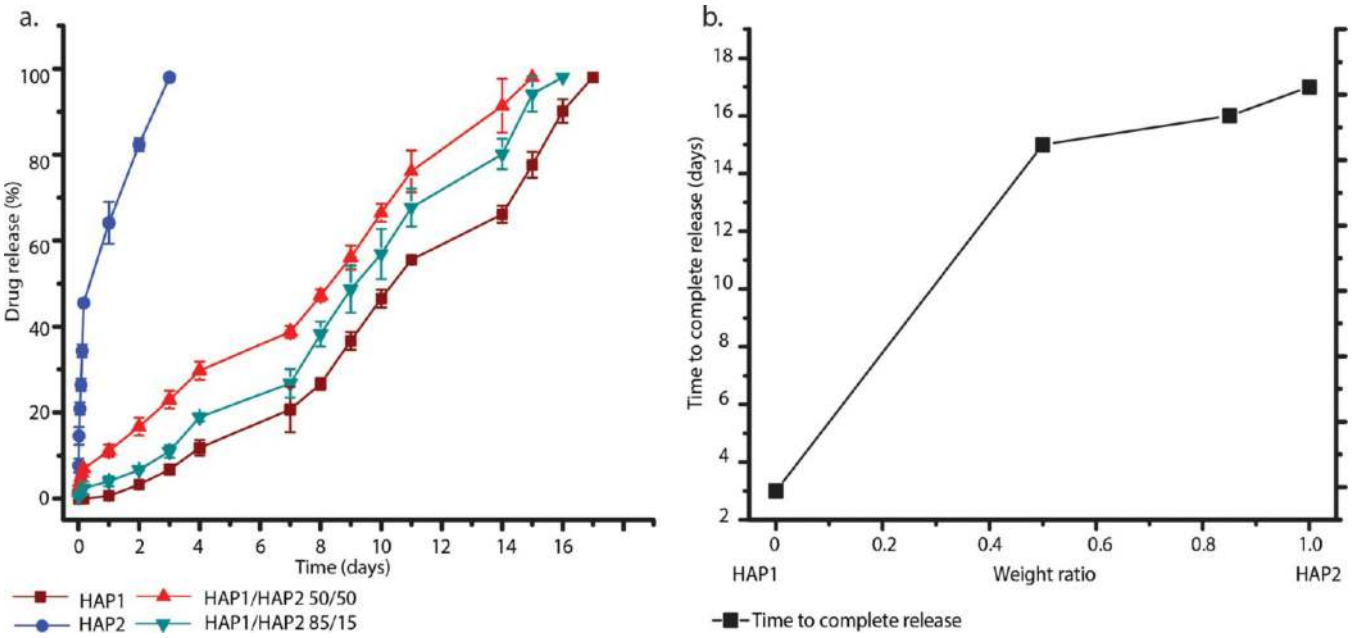

Figure 8.

(a) Ciprofloxacin release profiles of cements composed of HAP1 and HAP2 alone and HAP1 and HAP2 admixed in 85/15 and 50/50 weight ratios. Data are shown as averages with error bars representing standard deviation. (b) Time to complete release of ciprofloxacin from the same four types of cements as in (a).

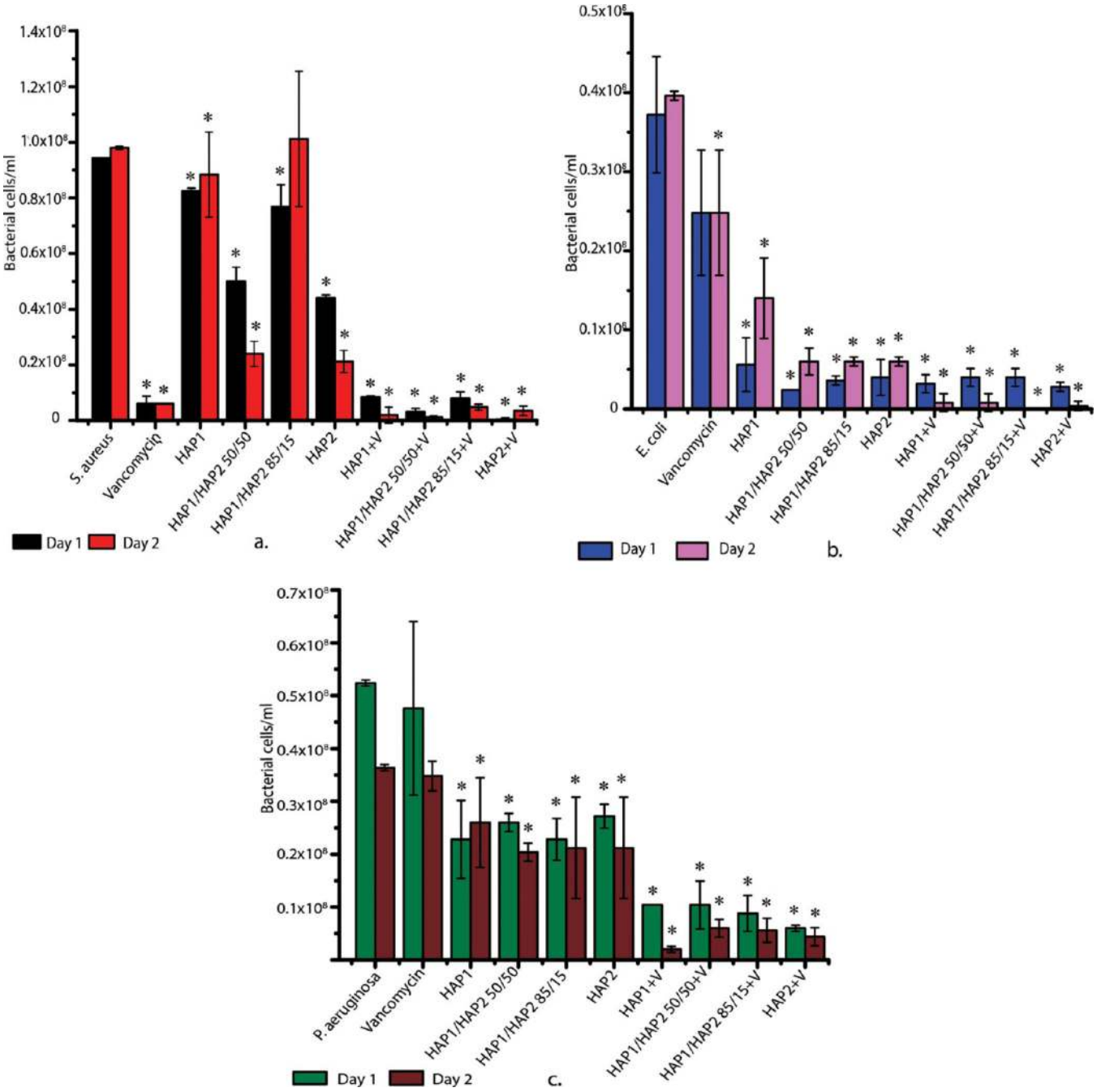

Figure 9.

Bacterial populations in a liquid inoculation assay of bone cements alone and bone cements releasing vancomycin (+V). The assay was run after 24 and 48 h against (a) *S. aureus*, (b) *E. coli*, and (c) *P. aeruginosa*. Data are shown as averages with error bars representing standard deviation. Data points significantly different from the untreated control (far left, $p < 0.05$) are topped with a star.

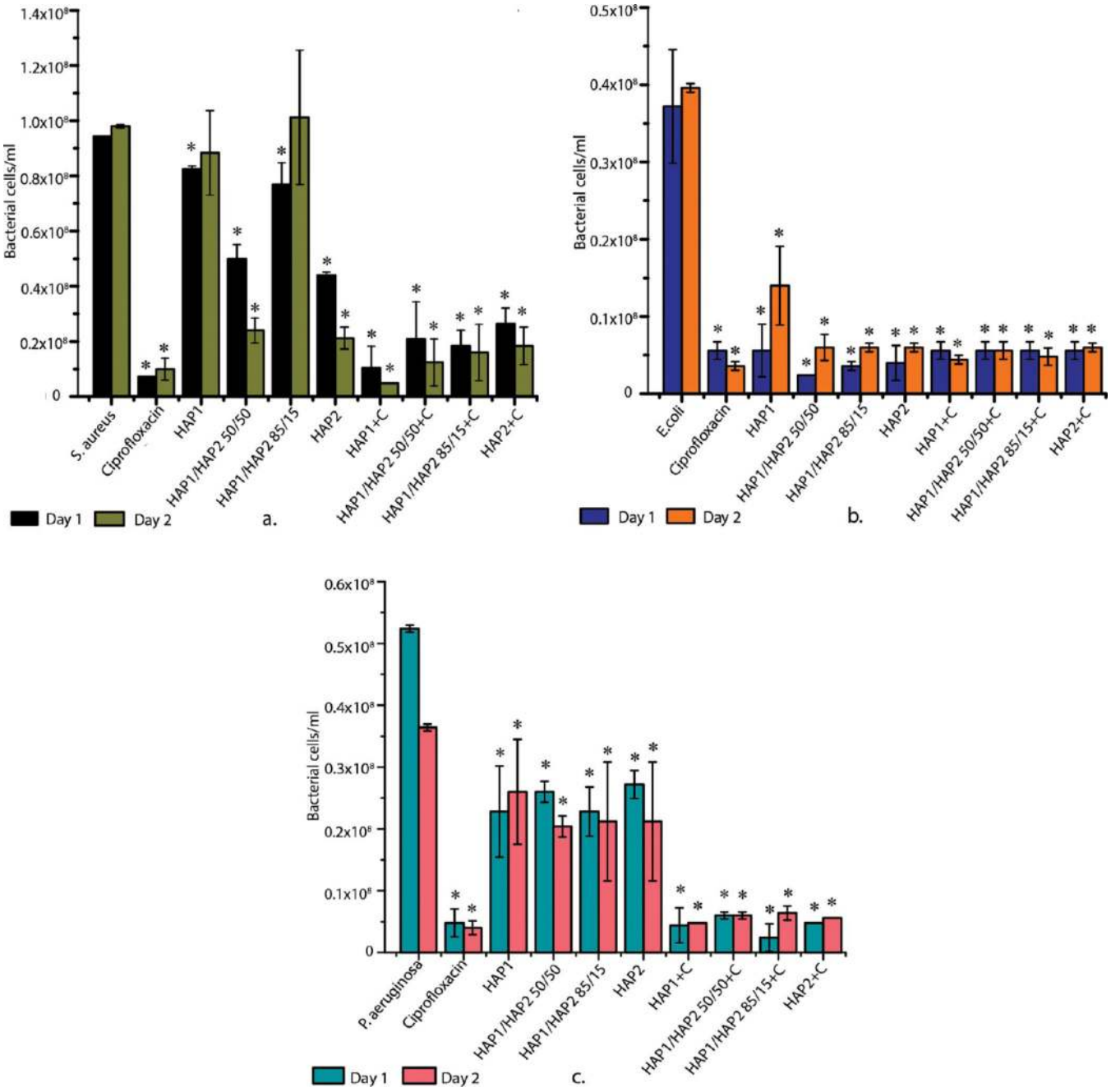

Figure 10.

Bacterial populations in a liquid inoculation assay of bone cements alone and bone cements releasing ciprofloxacin (+C). Assay was run after 24 and 48 h against (a) *S. aureus*, (b) *E. coli*, and (c) *P. aeruginosa*. Data are shown as averages, and error bars represent standard deviation. Data points significantly different from the untreated control (far left, $p < 0.05$) are topped with an asterisk (*).

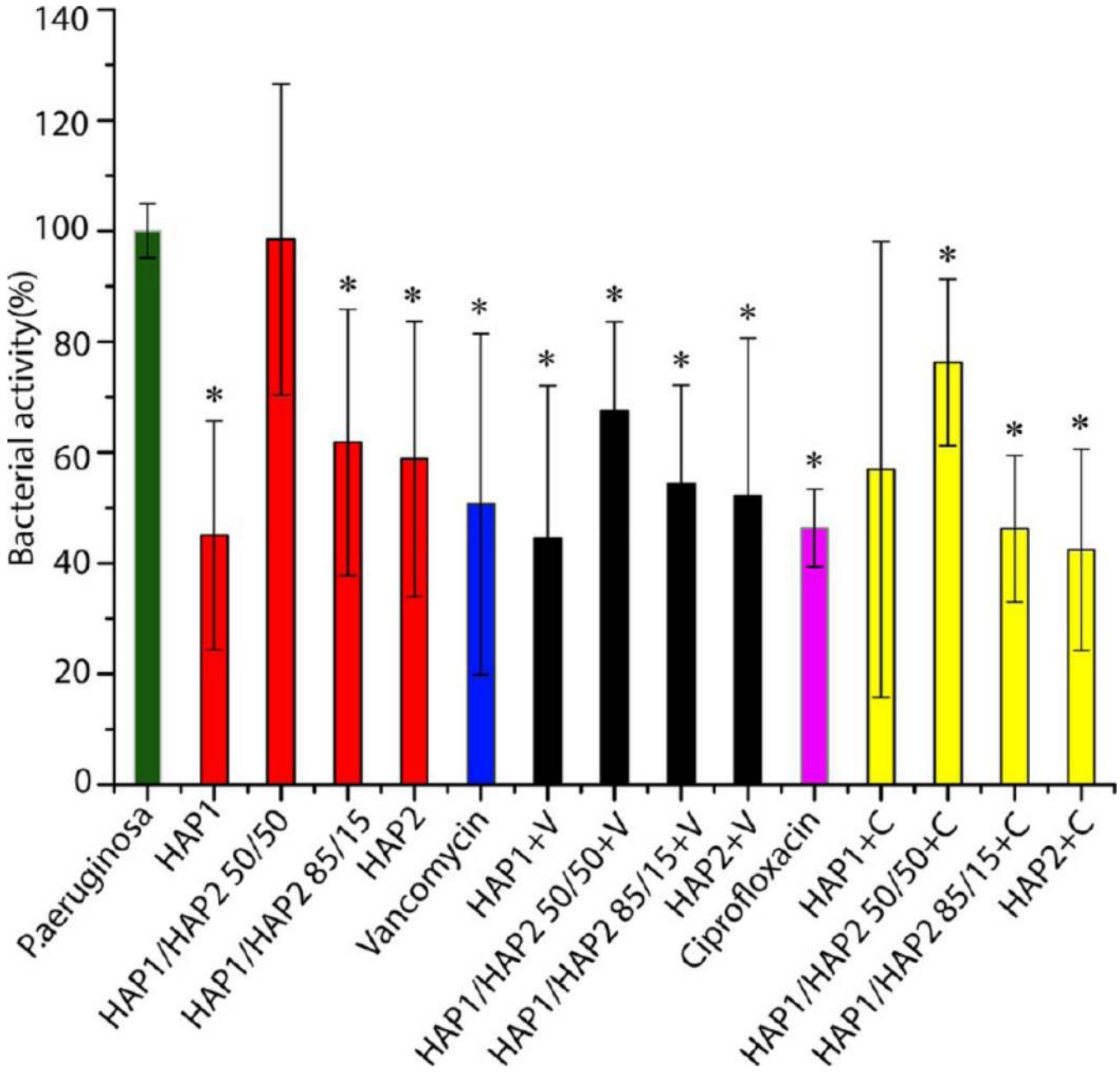

Figure 11.

Bacterial populations observed in an in vitro antibiofilm assay of bone cements alone and bone cements loaded with vancomycin (+V) and ciprofloxacin (+C) after 24 h of incubation with *P. aeruginosa* biofilm. Data are shown as averages, and error bars represent standard deviation. Bacterial activities significantly different from the untreated control (*P. aeruginosa*, $p < 0.05$) are topped with an asterisk (*).

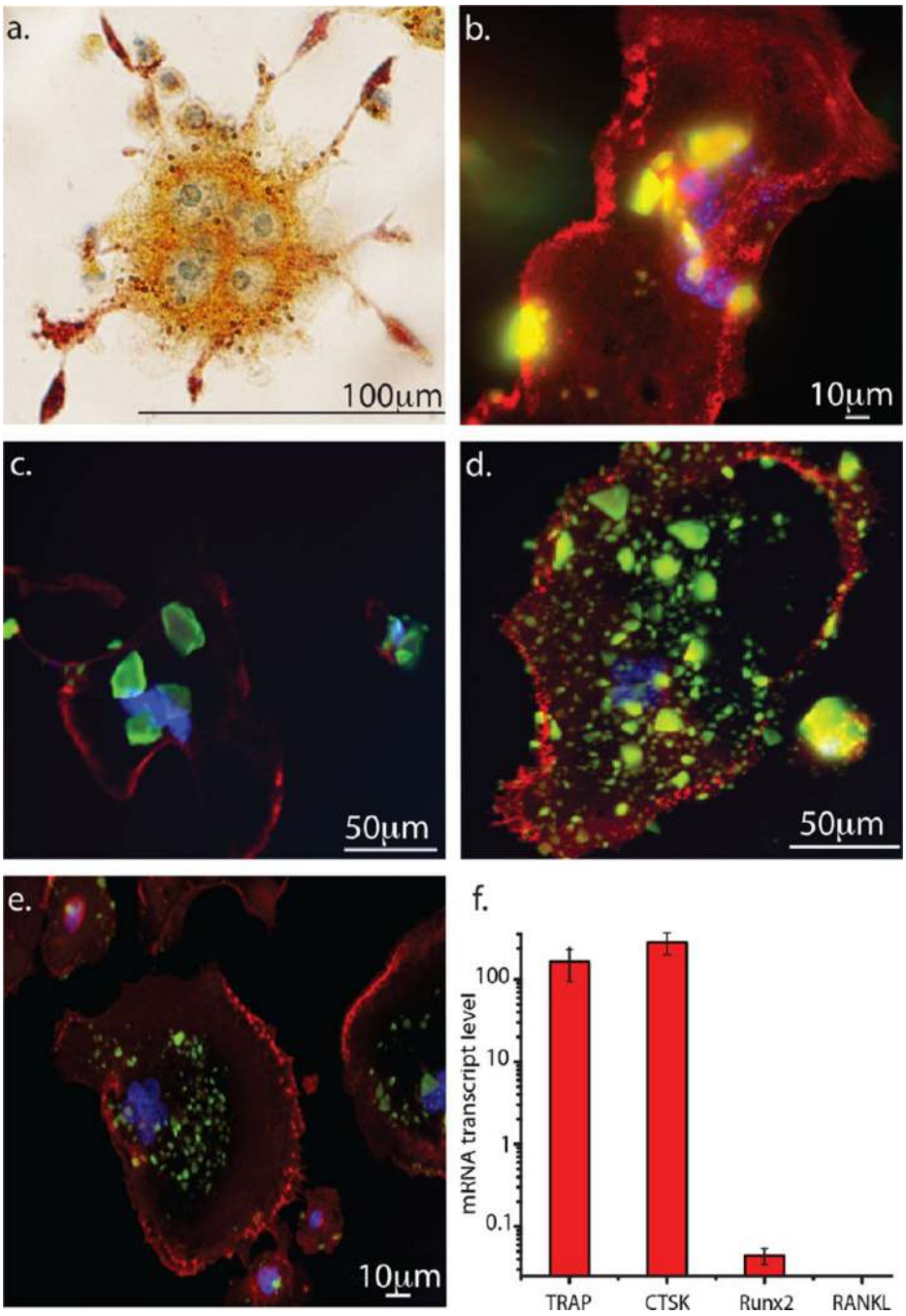

Figure 12.

Fluorescent optical micrographs showing the multinucleated morphology of (a) a TRAP-stained RAW264.7 cell differentiated into an osteoclastic phenotype and the interaction of osteoclastic RAW264.7 cells with (b) HAP1, (c) HAP1/HAP2 50/50, (d) HAP1/HAP2 85/15, and (e) HAP2 cements. The images show the multinucleated structure of osteoclastic cells and the resorption of a large number of cement particles. (f) qPCR gene expression analysis of osteoclastic markers TRAP and CTSK and of osteoblastic markers Runx2 and RANKL in differentiated RAW264.7 cells.

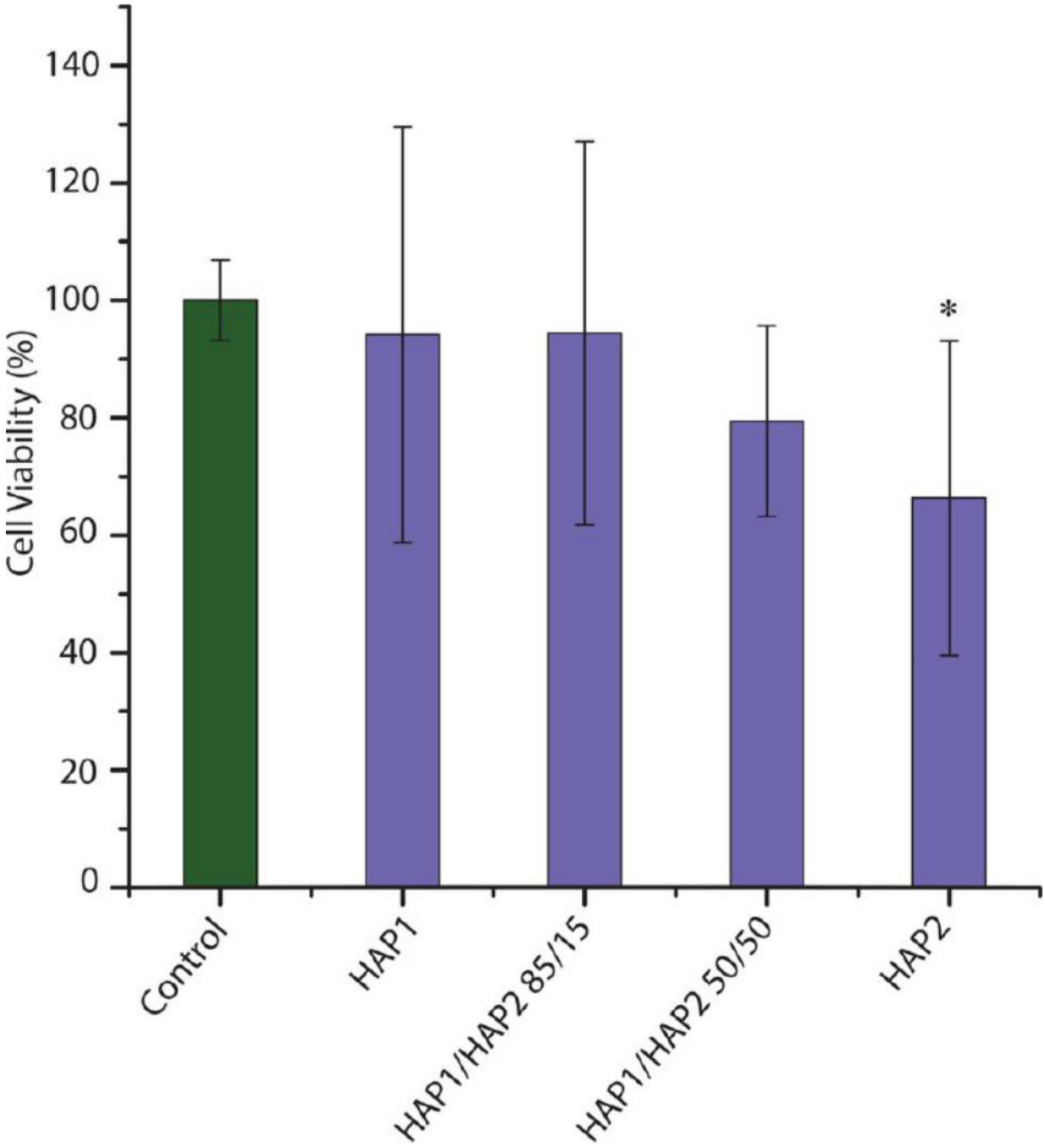

Figure 13.

Cell viability after a 48 h treatment of osteoblastic MC3T3-E1 cells with the cement samples determined using MTT assay. Absorbance of all the samples was normalized to the optical density of the negative control measured at $\lambda = 540$ nm. Cell viabilities significantly different with respect to the control group ($p < 0.05$) are marked with an asterisk (*).

Table 1

Composition of the Solid Phase of the Synthesized Drug-Loaded Cement Samples

cement sample	HAP1 (g)	HAP2 (g)	HAP3 (g)	drug (g)
HAP1	0.8	0	0	0.02
HAP1/HAP2 50/50	0.4	0.4	0	0.02
HAP1/HAP2 85/15	0.68	0.12	0	0.02
HAP2	0	0.8	0	0.02

Table 2

Porosities of HAP Cements

sample	porosity (%)
HAP1	42.6 ± 24.1
HAP1/HAP2 50/50	51.3 ± 21.3
HAP1/HAP2 85/15	46.9 ± 22.4
HAP2	54.9 ± 22.8

Table 3

Results of the Agar Diffusion Assay of Bone Cement Samples Containing Vancomycin and Ciprofloxacin